Biochem. J. (2013) **451**, 329–342 (Printed in Great Britain) doi:10.1042/BJ20121871

multimedia online data

Adenosine-binding motif mimicry and cellular effects of a thieno[2,3-*d*]pyrimidine-based chemical inhibitor of atypical protein kinase C isoenzymes

Svend KJÆR*[1], Mark LINCH†[1], Andrew PURKISS*, Brenda KOSTELECKY*†, Phillip P. KNOWLES*, Carine ROSSE†, Philippe RIOU†, Christelle SOUDY‡, Sarah KAYE‡, Bhavisha PATEL‡, Erika SORIANO*, Judith MURRAY-RUST*, Caroline BARTON‡, Christian DILLON‡, Jon ROFFEY‡, Peter J. PARKER†§[2] and Neil Q. McDONALD*‖[2]

*Structural Biology, Cancer Research UK, 44 Lincoln's Inn Fields, London WC2A 3LY, U.K., †Protein Phosphorylation Laboratories, Cancer Research UK, 44 Lincoln's Inn Fields, London WC2A 3LY, U.K., ‡Cancer Research Technology Discovery Laboratories, Wolfson Institute for Biomedical Research, University College London, Gower Street, London WC1E 6BT, U.K., §Division of Cancer Studies, King's College London, New Hunts House, Guy's Campus, London SE1 1UL, U.K., and ‖Institute of Structural and Molecular Biology, Department of Biological Sciences, Birkbeck College, University of London, Malet Street, London WC1E 7HX, U.K.

The aPKC [atypical PKC (protein kinase C)] isoforms ι and ζ play crucial roles in the formation and maintenance of cell polarity and represent attractive anti-oncogenic drug targets in Ras-dependent tumours. To date, few isoform-specific chemical biology tools are available to inhibit aPKC catalytic activity. In the present paper, we describe the identification and functional characterization of potent and selective thieno[2,3-*d*]pyrimidine-based chemical inhibitors of aPKCs. A crystal structure of human PKCι kinase domain bound to a representative compound, CRT0066854, reveals the basis for potent and selective chemical inhibition. Furthermore, CRT0066854 displaces a crucial Asn-Phe-Asp motif that is part of the adenosine-binding pocket and engages an acidic patch used by arginine-rich PKC substrates. We show that CRT0066854 inhibits the LLGL2 (lethal giant larvae 2) phosphorylation in cell lines and exhibits phenotypic effects in a range of cell-based assays. We conclude that this compound can be used as a chemical tool to modulate aPKC activity *in vitro* and *in vivo* and may guide the search for further aPKC-selective inhibitors.

Key words: ATP pocket, atypical protein kinase C, cell-based assay, cell migration, cell polarity, chemical inhibitor, crystallography, Madin–Darby canine kidney (MDCK) cell, protein kinase A/protein kinase G/protein kinase C family kinase (AGC kinase).

INTRODUCTION

PKC (protein kinase C) isoenzymes are an important family of serine/threonine protein kinases that contribute to many diverse cellular and tissue functions, as well as human disease pathologies including cancer development and progression [1,2]. The molecular architecture of PKC family members is conserved throughout the cPKC (classical PKC; cPKCα, cPKCβ and cPKCγ), nPKC (novel PKC; nPKCδ, nPKCε, nPKCη and nPKCθ) and aPKC (atypical PKC; aPKCζ and aPKCι) isoforms. They all comprise a C-terminal serine/threonine protein kinase domain [belonging to the AGC kinase (protein kinase A/protein kinase G/PKC family kinase) superfamily] and an N-terminal regulatory domain [3]. The kinase domain has a C-terminal extension unique to AGC kinases that contain essential 'priming' phosphorylation sites required for catalytic activation [4]; in aPKCs, the most C-terminal of these is replaced by a phosphomimetic glutamate residue. The regulatory domain within all PKC isoforms has an inhibitory region (pseudo-substrate motif) and distinctive arrangements of C1, C2 and/or PB1 (Phox/Bem1) domains (the last being exclusive to the aPKCs) that together are crucial for conferring isoform-specific functions [3].

The aPKC isoforms (PKCζ and PKCι) diverge from other PKC family members as their regulatory domains are unresponsive to diacylglycerol, phosphatidylserine and Ca^{2+}. Instead they are regulated by protein interactions, for example with polarity proteins Par-6, Par-3 and the Rho family GTPase cdc42 [5]. These components assemble into an evolutionarily conserved Par-6–aPKC–Par-3 complex present in both invertebrates and vertebrates that controls apical–basal polarity in epithelial cells and anterior–posterior positioning in asymmetric cell division [6,7]. In addition to an established role in cell polarity, aPKC is required for normal cell proliferation, mitotic spindle orientation [8,9] and migration [10,11].

There has been considerable interest in aPKCs as drug targets due to their role in cancer development and progression [12]. In cancer-specific cell models, PKCζ is required for EGF (epidermal growth factor)-induced migration of human breast and lung cancer cells and CSF-1 (colony-stimulating factor 1) chemotaxis of macrophages and acute monocytic leukaemic cells [13–15]. PKCι promotes nicotine-induced migration and invasion of lung cancer cells via phosphorylation of m- and μ-calpains [16] and is required for non-adherent cell growth in a Rac-1-dependent manner [17]. The potential importance of aPKC in Her2-driven malignancies

Abbreviations used: Ade, adenosine-binding; AGC kinase, protein kinase A/protein kinase G/protein kinase C family kinase; aPKC, atypical protein kinase C; BIM-1, bisindolylmaleimide-1; CCD, charge-coupled-device; cPKC, classical protein kinase C; 2D, two-dimensional; 3D, three-dimensional; DCM, dichloromethane; DMEM, Dulbecco's modified Eagle's medium; DTT, dithiothreitol; F-actin, filamentous actin; FBS, fetal bovine serum; GFP, green fluorescent protein; GST, glutathione transferase; HEK, human embryonic kidney; HRP, horseradish peroxidase; HTS, high-throughput screen; IMAP, immobilized metal ion-affinity fluorescence polarization; LC, liquid chromatography; LLGL, lethal giant larvae; MDCK, Madin–Darby canine kidney; MI, mass ion; nPKC, novel protein kinase C; NRK, normal rat kidney cell; PKC, protein kinase C; PSAL, predominantly single apical lumen; RMSD, root mean square deviation; RNAi, RNA interference; RT, retention time; SPR, surface plasmon resonance; TLS, translation libration screw-motion.

[1] These authors contributed equally to this work.

[2] Correspondence may be addressed to either of these authors (email neil.mcdonald@cancer.org.uk or peter.parker@cancer.org.uk).

The structural co-ordinates for PKCι_k bound to CRT0066854 will appear in the PDB under the accession number 3ZH8.

was demonstrated when the aberrant polarity induced by forced Her2 dimerization in human mammary epithelial MCF-10A cells embedded in Matrigel™ was partially reversed following genetic disruption of aPKC binding to Par-6 [18]. In model organisms, aPKC has been shown to co-operate with *bona fide* oncogenes, including Ras and Notch in *Drosophila melanogaster*, to lead to invasive and metastatic tumours [19,20]. Furthermore, in transgenic mice K-Ras-induced lung cancer is reduced following depletion of PKCι or its adaptor protein p62 [21,22].

In human malignancy, one of the most frequent amplicons is 3q26, the location of the PKCι gene (HGNC symbol PRKCI). PKCι gene amplification leads to high protein levels and is correlated with poor clinical outcomes in squamous cell carcinomas of the lung [17] and oesophagus [23]. High PKCι expression has been correlated with poor prognosis and/or worse stage in an increasing number of human cancers including breast [24], pancreas [25], stomach [26], bile duct [27] and brain [28]. In addition to the compelling evidence for a role of PKCι in human malignancy, the interest in PKCι as a therapeutic target was further enhanced by the finding that elevated PKCι protein is associated with chemotherapy resistance [29] and that depletion/inhibition of PKCι is synergistic with some conventional chemotherapies [30–32].

Like many protein kinases, aPKC isoenzymes are amenable to small-molecule chemical inhibition either through their ATP-binding clefts or allosteric pockets [33]. However, there are few selective chemical biology tools to inhibit aPKC catalytic activity. Available tools include the non-selective and relatively impotent BIM-1 (bisindolylmaleimide 1), Gö6983 and Gö6976 compounds or a PKCζ pseudo-substrate peptide containing a membrane-targeting myristoylation site [34]. The development of effective ATP-competitive inhibitors against aPKCs, similar to other protein kinases, has been complicated by challenges in both potency and selectivity [33]. In general, such inhibitors acquire selectivity by associating with both the ATP-binding site and with adjacent residues, which are less well conserved. Other approaches include screening for allosteric inhibitors of PKCζ that target the PIF pocket [35] or blocking PKCι interaction with Par-6, for example with ATM (aurothiomalate), a quite different class of PKCι inhibitor which exhibits potent antitumour activity in lung cancer [36].

In the present study, we report the identification of an aPKC inhibitor CRT0066854 which is able to mimic both ATP and a key side chain that forms part of the aPKC nucleotide-binding cleft. We define the compound's mechanism of action by crystallographic and biochemical methods and demonstrate its utility through the use of phenotypic cell-based assays. Together, our data indicate that CRT0066854 is a potent and selective chemical tool to modulate aPKC activity both *in vitro* and in cells.

EXPERIMENTAL

Chemical synthesis of CRT0066854 and CRT0066390

Synthesis of (*S*)-N*1*-(2-pyridin-4-yl-5,6,7,8-tetrahydro-benzo[4,5]thieno[2,3-*d*]pyrimidin-4-yl)-butane-1,2-diamine (CRT0066854)

*Synthesis of 2-pyridin-4-yl-5,6,7,8-tetrahydro-benzo[4,5]thieno[2,3-*d*]pyrimidin-4-ol (**A-1**)*

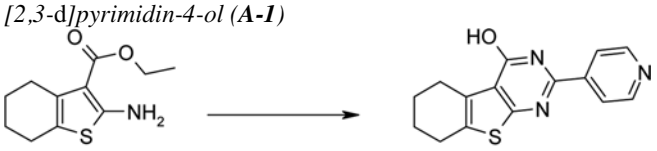

[A-1]

To a solution of 4-cyanopyridine (1.25 g, 12 mmol) in dry dioxane (10 ml) was added 2-amino-4,5,6,7-tetrahydro-benzo[b]thiophene-3-carboxylic acid ethyl ester (2.25 g, 10 mmol) followed by potassium-tert-pentylate 1.7 M in toluene (12 ml, 20 mmol). The reaction mixture was stirred at room temperature (20 °C) overnight. After completion the precipitate formed was filtered and washed with diethyl ether. The residue was used without any further purification in the next step. LC (liquid chromatography)–MS method: RT (retention time): 3.54 min, MI (mass ion): 284 [$M+1$]. ^{1}H NMR (300 MHz, DMSO): 8.56 (d, 2 H), 8.12 (d, 2 H), 2.90 (m, 2 H), 2.67 (m, 2 H), 1.76 (m, 4 H).

*Synthesis of 2,4,6-tri-isopropyl-benzenesulfonic acid 2-pyridin-4-yl-5,6,7,8-tetrahydro-benzo[4,5]thieno[2,3-*d*]pyrimidin-4-yl ester (**A-2**)*

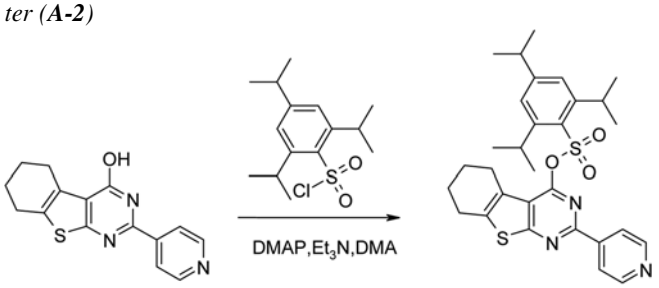

[A-1] [A-2]

To a solution of 2-pyridin-4-yl-5,6,7,8-tetrahydro-benzo[4,5]thieno[2,3-*d*]pyrimidin-4-ol (1 g, 3.5 mmol) (**A-1**) in DCM (dichloromethane, 10 ml) was added 2,4,6-tri-isopropylbenzenesulfonyl chloride (1.3 g, 4.2 mmol), triethylamine (Et_3N) (1.5 ml, 10.5 mmol) and DMAP (4-dimethylaminopyridine) (6 mg, 0.05 mmol). The mixture was stirred at room temperature for 1 h. After completion the mixture was diluted with water and the product was extracted into DCM (2×2 ml). The combined extracts were dried with magnesium sulfate, filtered and evaporated under reduced pressure to yield the title compound as a brown solid, which was used without further purification in the next step. LC–MS method: RT: 6.23 min, MI: 550 [$M+1$].

Synthesis of (S)*-3-phenyl-propane-1,2-diamine (**A-3**)*

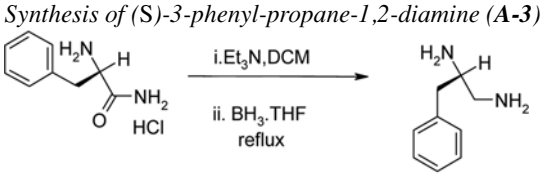

[A-3]

To a suspension of (*S*)-2-amino-3-phenyl-propionamide hydrochloride (540 mg, 2.7 mmol) in DCM (5 ml) was added triethylamine (Et_3N) (380 μl, 2.7 mmol). The suspension was stirred for 2 h at room temperature, the resulting solid was filtered and the filtrate was concentrated under reduced pressure to yield a white solid, to which was added dropwise a 1 M solution of BH_3 in THF (tetrahydrofuran, 20 ml, 20 mmol), the solution was stirred overnight at reflux. After cooling the solution was hydrolysed by slow addition of an excess of 10 % acetic acid/methanol (30 ml) and refluxed for a further 2 h. The solvent was removed under reduced pressure, and the residue was dissolved in methanol and passed through a SCX-2 cartridge and washed with methanol. The product was released from the cartridge using a solution of 2 M ammonia/methanol. The solvent was evaporated to provide the title compound as a white solid which was used in the next step without further purification. LC–MS method: RT: 0.36 min, MI: 151 [$M+1$].

*Synthesis of (*S*)-N*1*-(2-pyridin-4-yl-5,6,7,8-tetrahydro-benzo [4,5]thieno[2,3-*d*]pyrimidin-4-yl)-butane-1,2-diamine (**Compound A**, CRT0066854)*

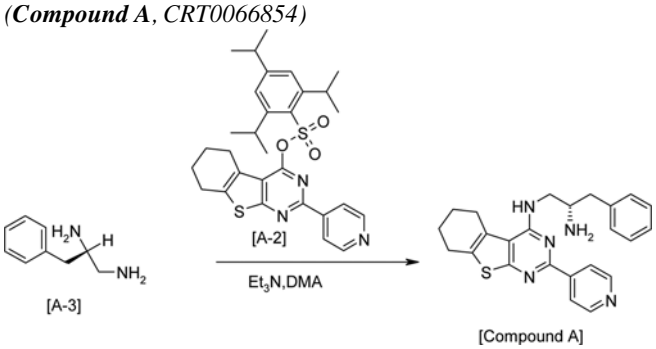

To a solution of 2,4,6-tri-isopropyl-benzenesulfonic acid 2-pyridin-4-yl-5,6,7,8-tetrahydro-benzo[4,5]thieno[2,3-*d*] pyrimidin-4-yl ester (**A-2**) (100 mg, 0.180 mmol) in DMA (dimethylacetamide, 2 ml) was added (*S*)-3-phenyl-propane-1,2-diamine (**A-3**) (30 mg, 0.180 mmol) followed by triethylamine (Et_3N) (50 μl, 0.36 mmol), the mixture was stirred at room temperature for 2 h. After completion the mixture was loaded on to a SCX-2 cartridge and washed with methanol. The product was released from the cartridge using a solution of 2 M ammonia/methanol. The ammonia/methanol eluent was concentrated under reduced pressure and the crude product was purified by preparative HPLC to yield the title compound. LC–MS method: 4, RT: 2.51 min, MI: 416 [$M + 1$]. ^{1}H NMR (300 MHz, DMSO): 8.64 (d, 2 H), 7.95 (d, 2 H), 7.36 (m, 5 H), 3.92 (m, 2 H), 3.46 (m, 2 H), 2.92 (m, 1 H), 2.91 (m, 2 H), 2.79 (m, 2 H), 1.83 (m, 4 H).

*Synthesis of (*R*)-N*1*-(2-pyridin-4-yl-5,6,7,8-tetrahydro-benzo[4,5]thieno[2,3-*d*]pyrimidin-4-yl)-butane-1,2-diamine (**Compound B**, CRT0066390)*

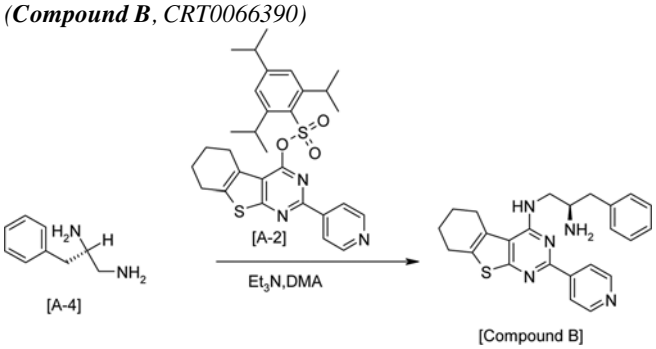

(*R*)-N*1*-(2-pyridin-4-yl-5,6,7,8-tetrahydro-benzo[4,5]thieno[2,3-*d*]pyrimidin-4-yl)-butane-1,2-diamine (**Compound B**, CRT0066390) was prepared from (*R*)-3-phenyl-propane-1,2-diamine (**A-4**) and 2,4,6-tri-isopropyl-benzenesulfonic acid 2-pyridin-4-yl-5,6,7,8-tetrahydro-benzo[4,5]thieno[2,3-*d*]pyrimidin-4-yl ester (**A-2**) to yield the title compound. LC–MS method: RT: 2.54 min, MI: 416 [$M + 1$]. ^{1}H NMR (300 MHz, DMSO): 8.74 (d, 2 H), 7.15 (d, 2 H), 7.34 (m, 5 H), 3.90 (m, 2 H), 3.52 (m, 2 H), 2.95 (m, 1 H), 2.94 (m, 2 H), 2.79 (m, 2 H), 1.83 (m, 4 H).

The tricyclic thienopyrimidine compound ASN2993118 (2-pyridin-4-yl-5,6,7,8-tetrahydro-benzo[4,5]thieno[2,3-*d*]pyrimidin-4-ylamine) was purchased directly from Asinex.

Plasmids

For mammalian studies, human PKCι cDNA (GenBank® accession number NM_002740.5), a gift from T. Biden (Garvan Institute of Medical Research, Australia), was subcloned into pEGFP-C1 vector (Clontech) using 5′-SalI and 3′-BamHI restriction sites. The cDNA contains two start codons at bp 1–3 and bp 28–30 with the second methionine residue denoted as the first amino acid of the protein. LLGL2 (lethal giant larvae 2) cDNA (GenBank® accession number NM_004524.2), a gift from T. Pawson (Samuel Lunenfeld Research Institute, ON, Canada), was subcloned into pEGFP-C1 with and without a 5′ FLAG-tag sequence using 5′-BamH1 and 3′-Sal1 restriction sites. For biochemical and structural studies, the kinase domain of PKCι (residues 239–587) was inserted into a pBacPAK-His3 vector (Clontech) using BamHI and XhoI restriction sites. The vector was modified to have a GST (glutathione transferase) followed by a 3C protease cleavage site upstream of the kinase domain. A C586S mutation was also introduced into the kinase domain using QuikChange® (Stratagene) according to the manufacturer's instructions in order to avoid oxidative cross-linking during crystallization.

PKCι_k and PKCι protein expression and purification

Recombinant baculoviruses used for infection were obtained using standard protocols (Oxford Expression Technologies). High Five cells were grown in shaker flasks in SFIII medium (Life Technologies) and 10 μg/ml gentamycin (Life Technologies). High Five cells were infected with recombinant baculoviruses at a multiplicity of infection of 2. To increase the phosphorylation state of PKCι to the fully active form, High Five cells were co-infected with PDK-1 baculovirus at a multiplicity of infection of 1. High Five cells were harvested 72 h post-infection and resuspended in lysis buffer {20 mM Hepes (pH 7.4) (Sigma), 150 mM NaCl (Sigma), 10 mM benzamidine (Sigma), 0.2 mM AEBSF [4-(2-aminoethyl)benzenesulfonyl fluoride] (Melford Laboratories), 1 mM EDTA (Sigma) and 1 mM DTT (dithiothreitol; Melford Laboratories)}. All purification steps were carried out at 4 °C or on ice. Cells were lysed by sonication and spun down at 30000 ***g*** for 30 min. PKCι_k or PKCι were purified using glutathione–Sepharose 4B beads (Amersham Biosciences), followed by removal of the GST affinity tag with GST-3C protease (PreScission Protease, Amersham Bioscience) and ion-exchange chromatography (Hi-Trap Q column, GE Healthcare). The protein was dialysed into the final buffer [25 mM Tris (pH 8.0), 150 mM NaCl, 1 mM EDTA and 1 mM DTT] and concentrated before use.

High-throughput screening and selectivity screens

We performed a small molecule HTS (high-throughput screen) against recombinant PKCι_k with confirmed hits profiled against recombinant PKCζ_k to verify pan-aPKC inhibition. We screened a 56000 CRT (Cancer Research Technology) chemical library collection at a single concentration of 30 μM [IMAP (immobilized metal ion-affinity fluorescence polarization) format, Molecular Devices]. The 56000 compounds comprises 46000 from a diverse collection and 10000 from a kinase-focused collection (including in-house compounds). The HTS assay used 10 pM PKCι and 100 nM 5FAM (fluorescein-amidite)-ERMRPRKRQGSVRRRV-NH_2 peptide and 30 μM ATP in a buffer consisting of 20 mM Hepes (pH 7.5), 10 mM $MgCl_2$, 1 mM DTT and 0.25 mM EGTA. The PKCι_k K_m for ATP was determined to be 30 μM using this IMAP assay. We used an isoquinoline sulfonamide H-series compound H-9 as the assay standard ($IC_{50} = 2$ μM). All final Z'-factors were greater than 0.5 and most were above 0.6. The H-9 assay standard inhibition at 2 μM gave 46.7 $\pm$ 4.8 % inhibition of PKCι_k activity. Hits from the HTS screen gave IC_{50} values from 0.2 to 30 μM. The initial hit rate was unusually low for a kinase HTS at 0.2 % with no confirmed hits arising from the kinase-focused subset

of our library. As the HTS used a truncated form of PKCι, we profiled our hits against the full-length human PKCι. The tricyclic thienopyrimidine ASN2993118 demonstrated activity against both full-length and the kinase domain of PKCι (as well as the kinase domain of PKCζ). Further validation of PKCι inhibitory activity was undertaken in orthogonal assay formats with ASN2993118, and mechanistically it was shown to have an ATP-competitive mode of inhibition. These studies confirmed ASN2993118 as a *bona fide* hit, and it was progressed into lead identification. Lead identification involved assaying modifications to the C^4 position of the central pyrimidine ring of ASN2993118. The Millipore KinaseProfiler™ service (Millipore) was used to determine the selectivity of CRT0066854 against a panel of kinases. This service used a radiometric assay and 1 μM single-point concentrations of CRT0066854. An ATP concentration of 30 μM (equivalent to the K_m of PKCι_k) was used.

In vitro kinetic assays for PKCι and IC_{50} determinations

The ADP Quest kit (DiscoveRx) was used to determine the k_{cat} and K_m values for fully primed phospho-species of PKCι_k, PKCζ_k and the nPKC isoform PKCε_k as a positive control (Supplementary Table S1 at http://www.biochemj.org/bj/451/bj4510329add.htm). This assay uses a coupled reaction to convert ADP into a product that has a fluorescence excitation at 530 nm and emission at 590 nm. Two synthetic peptides, a model substrate peptide (ERMRPRKQGSVRRRV) derived from PKCε and human LLGL2 substrate peptide (LKKSLRQSFRRMRR). For the k_{cat} (app) and K_m (app) reactions, the ATP concentration ranged from 0 to 200 μM while the synthetic peptide substrates were kept constant at 200 μM to avoid product inhibition. PKC isoenzyme concentrations were 5 nM for all three isoenzymes. The reactions were measured every 2 min for 30 min in a 384-well plate using a Safire^2 plate reader (Tecan). For determination of IC_{50} values, reactions were prepared using 20 μM ATP and 20 μM model substrate peptide. Protein concentrations were the same as indicated in the previous paragraph. Serial dilutions of inhibitors with concentrations ranging from 1 nM to 100 μM were added and fluorescence intensity was measured in end point assay mode.

SPR (surface plasmon resonance) measurements for CRT0066854 binding to PKCι_k

To conduct SPR measurements to obtain affinity and on and off rates for the inhibitor, we immobilized an anti-GST antibody (GEHC GST-capture kit) by amine coupling using standard protocols in flow cells 1 and 2. We then captured GST-tagged PKCι_k in flow cell 2 using 25 μg/ml in running buffer, 180 s, 5 μl/min. The running buffer consisted of 50 mM Tris, 150 mM NaCl, 10 mM $MgCl_2$, 1 mM $MnCl_2$, 1 mM DTT and 0.05 % P20 at pH 7.5. A GST control was captured in flow cell 1 using 25 μg/ml in the same running buffer (180 s, 5 μl/min). Then we ran a concentration series of inhibitor CRT0066854 over the captured PKCι_k. Concentrations used were 0, 16.125, 32.25, 62.5, 125, 250, 500, 1000, 1500 and 2000 nM.

Crystallography and structure determination

Crystals of PKCι_k bound to CRT0066854 were obtained at 20 °C using 200 nl drops formed by 100 nl of protein solution in 20 mM Tris (pH 7.5), 150 mM NaCl and 2 mM DTT buffer (containing a 5-fold molar excess of CRT0066854), mixed with 100 nl of precipitant solution containing 0.2 M ammonium iodide and 20 % (v/v) PEG3350 [poly(ethylene glycol) 3350]. Crystals were cryoprotected using 20 % ethylene glycol. Diffraction data were collected at Diamond [beamline IO3, at a wavelength of 0.92 Å (1 Å = 0.1 nm)] and processed with the CCP4 (collaborative computational project 4) software [37]. Molecular replacement was performed using the program Phaser [38], using the protein structure of PKC$_{\iota k}$ bound to BIM-1 (PDB code 1ZRZ) as a search model. Refinement was carried out with Phenix [39], using torsion angle NCS (non-crystallographic symmetry) and TLS (translation libration screw-motion; with three TLS groups per protein chain) parameters. For a summary of the crystallographic data, see Table 3. There are three molecules within the asymmetric unit, denoted A, B and C, with RMSDs (root mean square deviations) between Cα atoms A–B 0.13 Å for 321 pairs, A–C 0.13 Å for 312 pairs and B–C 0.19 Å for 314 pairs. Missing regions in the final model due to poor or non-existent electron density included residues 448–455 and 543–551. These residues belong to an aPKC-specific insert motif (residues 448–455) and the Ade (adenosine-binding) motif respectively. Selected well-defined water molecules were included together with two iodide ions. The position of the iodide ions was confirmed by inspection of an anomalous difference Fourier electron density map.

Cell culture

HEK (human embryonic kidney)-293, A549 and MDCK (Madin–Darby canine kidney) cells were obtained from Cell Production, Cancer Research UK (CRUK) and cultivated in DMEM (Dulbecco's modified Eagle's medium), 10 % FBS (fetal bovine serum) and penicillin–streptomycin (Invitrogen). HCT-116 cells were obtained from Cell Production, CRUK, and grown in McCoy's 5A medium with 10 % FBS and penicillin–streptomycin. NRK (normal rat kidney)-49F cells were a gift from Dr J. Camonis (Institut Curie, Paris, France) and have previously been characterized [10]. The cells were cultivated in DMEM and 10 % FBS under 5 % CO_2 conditions.

Antibodies

The following antibodies were used for immunoblotting: mouse monoclonal anti-PKCλ/ι antibody used at a 1:500 dilution (BD Biosciences), mouse monoclonal anti-α-tubulin antibody at a 1:10 000 dilution (Sigma), rabbit polyclonal anti-pLLGL1/2 antibody at a 1:500 dilution (Abnova), rabbit polyclonal anti-phospho-serine PKC substrate antibody used at a 1:500 dilution (Cell Signaling Technology; broad phospho-serine motif recognition for AGC kinase substrates) and rabbit polyclonal anti-GFP (green fluorescent protein) antibody used at a 1:1000 dilution (Santa Cruz Biotechnology). In ELISA, the anti-pLLGL1/2 antibody (Abnova) was used at a 1:1000 dilution and HRP (horseradish peroxidase)-conjugated goat anti-(rabbit IgG) antibody (Perbio Science) was used at a 1:2000 dilution.

Western blotting

For immunoblotting, lysates or immunoprecipitates were resolved using precast NuPAGE 4–12 % Bis-Tris gels (Invitrogen) and transferred on to nitrocellulose membranes (PROTRAN, Whatman). Immunoblots were blocked in 3 % BSA–TBST (Tris-buffered saline containing 0.1 % Tween 20) and probed with primary antibodies as indicated. Following incubation with species-specific HRP-conjugated secondary antibodies, bands were visualized radiographically.

Immunoprecipitation

After 36 h, transfected HCT-116 cells were lysed in lysis buffer [1 % Triton X-100, 20 mM Tris/HCl (pH 8), 130 mM NaCl, 1 mM

DTT, 10 mM sodium fluoride, complete EDTA-free protease inhibitor cocktail (Roche) and phosphatase inhibitor cocktails (set II + IV; Calbiochem)]. After centrifugation (13000 ***g***, 4 °C, 10 min), soluble proteins were precleared then incubated with anti-GFP magnetic beads (GFP–TRAP; Chromotek) for 90 min at 4 °C. Beads were washed five times with lysis buffer (containing 260 mM NaCl), then the bound proteins were eluted in Laemmli sample buffer, resolved by SDS/PAGE and analysed by immunoblotting. Where indicated, cells were treated for 2 h before lysis with DMSO (as a control), 10 μM BIM-1 (Calbiochem) or 5 μM Gö6983 (Calbiochem) or CRT0066854.

Transfection

Transient reverse transfections of cDNA for HEK-293 cells were performed on poly-L-lysine precoated plates using Lipofectamine™ 2000 as per the manufacturer's instructions (Invitrogen). Co-transfections of PKCι and LLGL2 were at a 4:1 DNA ratio. HCT-116 cells were transfected 24 h after plating using FuGENE® HD as per the manufacturer's instructions (Roche). The cells were then grown in normal medium for 36 h before further manipulations. In ELISA, HEK-293 cells were transfected with cDNA using JetPEI reagent as per the manufacturer's instructions (Autogen Bioclear).

ELISA

HEK-293 cells were transfected in a 10-cm dish as per the manufacturer's instructions (Corning). After 16 h, the cells were trypsinized and seeded into a 96-well plate at 1.5×10^4 cells/well and medium was replenished. After a further 24 h, the medium was replaced by new medium and a range of CRT0066854 inhibitor concentrations. After 1 h of inhibitor treatment, lysates were prepared using ice-cold Tris lysis buffer [150 mM NaCl, 20 mM Tris (pH 7.5), 1 mM EGTA, 1 mM EDTA and 1 % Triton X-100]. Lysates were transferred on to an anti-FLAG-coated ELISA plate (Sigma) and incubated for 2 h with gentle shaking, followed by an automated wash step (Tecan plate washer) with wash buffer [50 mM Tris (pH 7.5), 0.15 M NaCl and 0.02 % Tween 20]. The immunocomplexed protein was incubated with anti-pLLGL1/2 primary antibody overnight at 4 °C, followed by an automated wash and then addition of HRP-conjugated secondary antibody. After a further wash, 3,3′,5,5′-tetramethylbenzidine (Sigma) was added according to the manufacturer's instructions and attenuance was read at 450 nm using an Ascent plate reader (Thermo Labsystems).

Cell viability

CellTitre-Glo® (Promega) cell viability assay was carried out as per the manufacturer's instructions. The luminescent measurement of ATP was performed using the EnVision plate reader (PerkinElmer).

Soft agar assay

Single-cell suspension of HeLa cells were resuspended in 0.35 % agarose in RPMI 1640 medium and 10 % FBS at a density of 1500 cells/ml. The agarose–cell mixture (3 ml) was added to each 35-mm well that had been precoated with 1.5 ml of 0.5 % agarose. Plates were incubated at 4 °C for 20 min to allow the agarose to set before being placed in the 37 °C incubator for 10–14 days. Colonies were stained with 0.005 % Crystal Violet for 1 h, after which images were taken using a CCD (charge-coupled-device) camera and colony number was counted using ImageJ software version 1.40g.

3D (three-dimensional) cystogenesis assay

The 3D culture of MDCK cells in Matrigel™ was performed as follows: MDCK cells in exponential-phase growth were trypsinized and resuspended in standard medium, supplemented with 2 % low growth factor Matrigel™ (BD Biosciences) at 2×10^4 cells/ml. Each well of an eight-well chamber slide (BD Biosciences) was precoated with 30 μl of 100 % Matrigel™ to which 400 μl of the cell suspension was added. Inhibitors were added on day 1 and the medium of 2 % Matrigel™ in the presence or absence of inhibitor was changed on alternate days for 5 days.

Wound migration assay

Wounds were inflicted by scratching the cell surface with a plastic pipette tip. Images were recorded using a Nikon Eclipse Ti inverted videomicroscope and Coolsnap HQ2 camera (Photometrics). All inhibitor treatments were performed with 1 h pre-incubation. The migration speed was monitored by measuring the change in the area surrounding the wound over time, using Metamorph software. Statistical analysis (ANOVA 2 factors) were performed using Prism Software.

Immunofluorescence microscopy

MDCK cells grown in Matrigel™ on chamber slides were fixed with 2 % formaldehyde in PBS, washed in PBS and then permeablized with 0.5 % Triton X-100 in PBS. Following a further wash, cells were directly stained with Phalloidin Alexa Fluor® 546 (1:200 dilution; Invitrogen) and Hoechst dyes (1:5000 dilution; Invitrogen). After a quick rinse with PBS, the cultures were mounted with Prolong Gold hard-set mounting medium (Invitrogen).

MDCK cysts that had their F-actin (filamentous actin) stained with Phalloidin Alexa Fluor® 546 were visualized with a confocal microscope (Zeiss 510) and an apical lumen assessment was carried out. The middle of the cyst in the z-plane was identified and the following criteria were observed to determine whether the cyst had a 'predominantly single lumen': (i) a continuous F-actin-defined lumen; (ii) the luminal actin staining being more intense than the basal (outside) staining; (iii) a uni-dimensional measurement of the lumen being at least one-third of the cyst diameter; and (iv) the uni-dimensional measurement of the lumen being twice the size of any other luminal structure.

Statistical analysis

Enzyme kinetic constants for PKCι_k were determined by fitting the data to the Michaelis–Menten equation using the graphics program Prism (GraphPad Prism, version 5.0d, GraphPad Software). Differences between the treatment groups were assessed by ANOVA with a repeated measurement module using Prism statistical software. P values of <0.05 were regarded as significant. Dose–response curves and the calculation of the Geometric Mean IC_{50} values were performed in SARview software (IDPS, version 6.2).

RESULTS

Discovery of potent and selective chemical inhibitors of aPKCs

To identify molecules that inhibit PKCι, a 56000-compound diverse chemical library assembled by the CRT Discovery

Table 1 IC_{50} values for selected aPKC inhibitors

CRT0066854, CRT0066390 and ASN2993118 were compared against full-length (FL) aPKCι. PKCζ and ROCK2 kinase domain (KD) were used for CRT0066854, and CRT0066390 was used as a control. IC_{50} values are geometric mean values determined using five times the kinase K_m for ATP.

aPKC inhibitors	CRT0066854 (μM)	CRT0066390 (μM)	ASN2993118 (μM)
PKCι FL	0.132	2.5	26
PKCζ FL	0.623	7.1	–
ROCK2 KD	0.620	30	–

Laboratories was screened at 30 μM against a 10 pM biphosphorylated (i.e. fully primed) form of the PKCι kinase domain (residues 239–587, referred to hereafter as PKCι_k). The PKCι K_m for ATP was determined to be 30 μM (Supplementary Table S1). The screen employed an IMAP (Molecular Devices) assay using a fluorescein-amidite (FAM)-tagged PKCε-derived pseudo-substrate sequence containing an alanine-to-serine mutant (PSS; pseudo-substrate substrate) that we found to be an excellent PKCι substrate. The screen identified several compounds with potent anti-PKCι_k activity including a tricyclic thieno[2,3-*d*]pyrimidine ASN2993118 (Figure 1A, upper panel). This hit had an IC_{50} of 11 μM against PKCι_k and 26.3 μM against full-length PKCι. Counter screening against PKCζ_k showed the compound inhibited with an IC_{50} of 36.5 μM. The low-molecular mass and calculated lipophilicity of ASN2993118 made it an attractive starting point for optimization. Exploration of the activity landscape around the central pyrimidine ring of ASN2993118 led to the identification of compounds with a diamine side chain at the pyrimidine C^4 position that exhibited increased inhibitory activity. This included CRT0066854 in which the pyrimidine C^4 position was substituted with a S-3-phenyl-propane-1,2-diamine moiety (Figure 1A, lower panel).

To characterize CRT0066854 further, we used an ADP Quest™ assay (Discoverx) to generate dose–response curves for fully primed phosphospecies of PKCζ_k, PKCι_k and the nPKC isoform PKCε_k as a control. The k_{cat} and K_m kinetic constants were determined for PKCζ_k, PKCι_k and the nPKC isoform PKCε_k using the ADP Quest™ assay (Supplementary Table S1). CRT0066854 was used at 10 μM. We used the structurally unrelated PKC inhibitors BIM-1 (10 μM) and Gö6983 (5 μM) from commercial sources as positive controls. IC_{50} values for CRT0066854 against PKCζ_k and PKCι_k were 450 nM and 86 nM respectively (Figure 1B). Comparing the IC_{50} values measured for BIM-1 (PKCζ_k $IC_{50} = 9.1$ μM and PKCι_k $IC_{50} = 5.5$ μM), indicates that CRT0066854 is approximately 20-fold more potent for PKCζ_k and over 60-fold more potent for PKCι_k than BIM-1. A similar increase in potency is observed for CRT0066854 compared with Gö6983 (PKCζ_k $IC_{50} = 13.9$ μM and PKCι_k $IC_{50} = 10.7$ μM) (Figure 1B). Inhibition of the nPKCε_k by CRT0066854 is significantly weaker, with a 16-fold higher IC_{50} ($IC_{50} = 7.21$ μM) compared with PKCζ_k and more than 80-fold greater than the IC_{50} for PKCι_k. We then measured IC_{50} values for full-length PKCζ and PKCι, which gave 639 nM and 132 nM respectively, comparable with those obtained from isolated aPKC kinase domains. Since CRT0066854 has a chiral centre, we prepared its enantiomer CRT0066390 and measured its IC_{50} values against full-length PKCι and PKCζ. This showed only low levels of inhibition of aPKC isoenzymes by CRT0066390 (Table 1).

To examine the selectivity profile of CRT0066854 *in vitro*, the compound was tested at Millipore using the KinaseProfiler™ screening service (Millipore) against 106 protein kinases at a 1 μM inhibitor concentration, screened at the K_m for ATP (Table 2). This is a radiometric assay format used with each kinase. The selectivity score S(80) is the number of kinases inhibited by greater than 80 % at 1 μM compound/total number of kinases tested. For CRT0066854, the S(80) score is close to 0.02, which indicates a good kinase selectivity [40]. Moreover, the compound showed striking selectivity for aPKC over other PKC isoenzymes (Table 2).

To test whether there was selectivity of the tool compound between the PKC subclasses in cells, GFP-tagged cPKCα, nPKCε and aPKCι proteins were expressed in HCT-116 cells and the cultures were treated with CRT0066854 for 30 or 90 min. As a control we used BIM-1 and Gö6983 to potently inhibit full-length novel and cPKC isoenzymes expressed in this cell line (Supplementary Figure S1 at http://www.biochemj.org/bj/451/bj4510329add.htm). Immuno-complexes were immune-isolated through the GFP-tag and immunoblotted with an anti-phospho-serine-PKC substrate antibody. In CRT0066854-treated cells, the number of phosphorylated substrate bands apparent was significantly diminished for cells overexpressing PKCι, but not PKCα or PKCε, demonstrating aPKC specificity in cells (Figure 1C). Together, these data suggested that CRT0066854 would be a potent and selective chemical tool to modulate aPKC activity both *in vitro* and in cells.

Kinetics of CRT0066854 inhibitor binding to PKCι_k

To characterize the interaction of CRT0066854 in solution with purified recombinant PKCι_k protein, we used SPR on a BIACORE T200 to measure the kinetics and affinity of this inhibitor. GST-tagged PKCι_k was captured using anti-GST monoclonal antibody immobilized via amine coupling. Sensorgrams were fitted to a 1:1 Langmuir binding model and kinetics constants were obtained and an affinity constant of 340 nM was calculated from k_d/k_a (Figure 1D, upper panel). A binding isotherm was also fitted to a 1:1 steady-state binding model and an affinity of 870 nM was obtained in good agreement with the value derived from the rate constants (Figure 1D, lower panel).

Structural basis for CRT0066854 selectivity for the PKCι kinase domain

To understand both the selectivity and binding mode of CRT0066854 we determined the crystal structure of CRT0066854 bound to PKCι_k (Table 3). Crystals of PKCι_k bound to CRT0066854 contain three very similar PKCι_k molecules in the asymmetric unit that each have a single inhibitor bound within the ATP cleft. The overall PKCι_k conformation bears many of the hallmarks of an active AGC kinase conformation (Supplementary Figure S2 at http://www.biochemj.org/bj/451/bj4510329add.htm) except for the lack of bound magnesium and the absence of an ordered Ade motif as discussed below [41]. The CRT0066854 compound makes predominantly hydrophobic interactions within the PKCι nucleotide-binding cleft, as well as five hydrogen bonds, including a water-mediated hydrogen bond (Figures 2A and 2B). The fused tricyclic scaffold (cyclohexa[4,5]thieno[2,3-*d*]pyrimidine) makes hydrophobic contacts with the PKCι_k glycine loop, stabilizing a 'closed' conformation. This tricyclic ring system deviates significantly from planarity and is curved with a puckered cyclohexane ring (Figure 2A). The thieno-1 nitrogen of the pyrimidine ring makes a crucial hydrogen bond to the Thr^{386} side chain. The thieno[2,3-*d*]pyrimidine ring system also has two important substituents: (i) a pyridine substituent at position 2 and (ii) a (2-amino-3-phenylpropyl)(methyl)amine

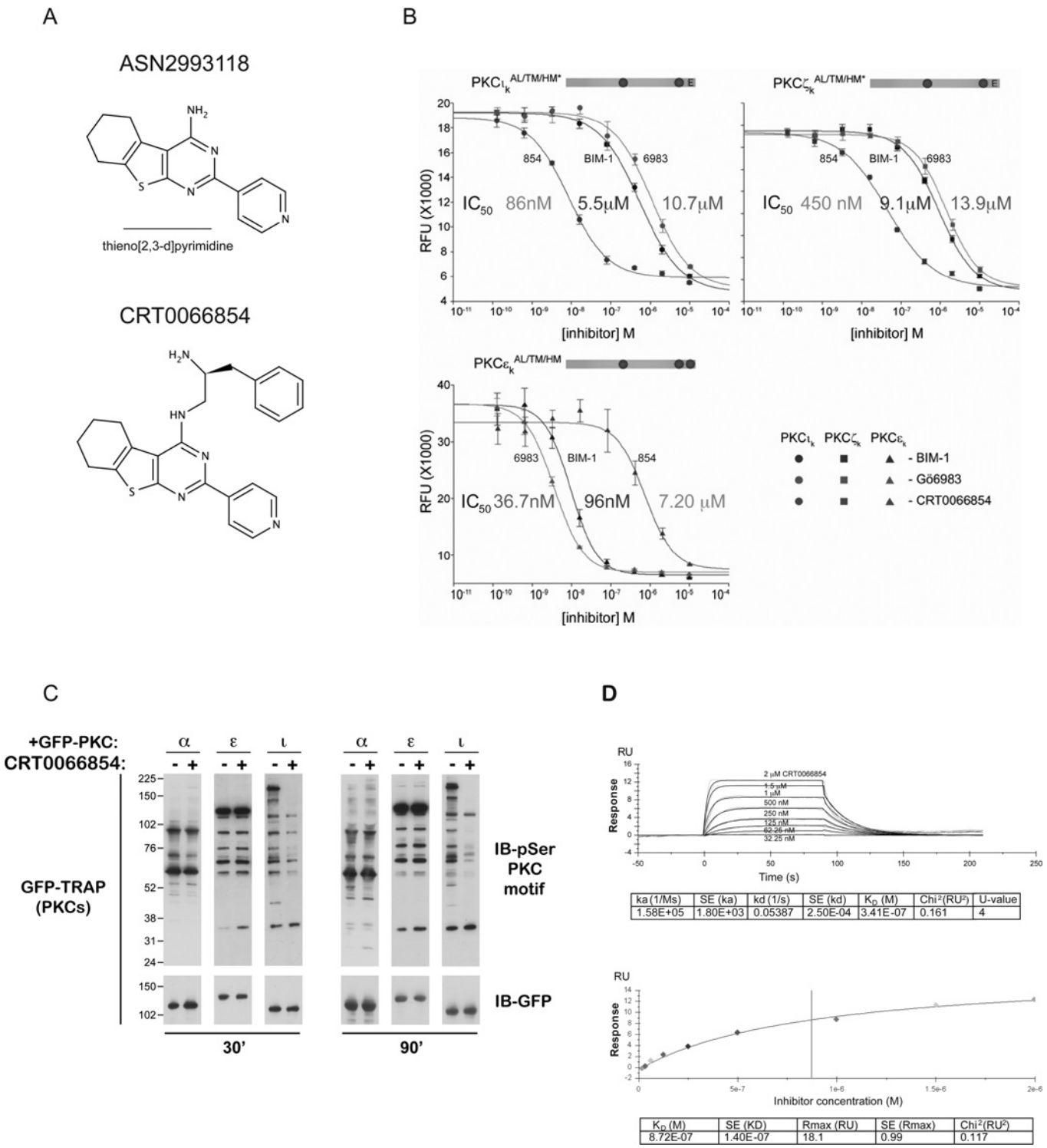

ka (1/Ms)	SE (ka)	kd (1/s)	SE (kd)	K_D (M)	Chi²(RU²)	U-value
1.58E+05	1.80E+03	0.05387	2.50E-04	3.41E-07	0.161	4

K_D (M)	SE (KD)	Rmax (RU)	SE (Rmax)	Chi²(RU²)
8.72E-07	1.40E-07	18.1	0.99	0.117

Figure 1 CRT0066854 selectively inhibits PKCζ and PKCι kinase activity *in vitro* and in cells

(**A**) Upper panel, chemical structure of the initial hit thieno[2,3-*d*]pyrimidine ASN2993118. Lower panel, chemical structure of compound CRT0066854. (**B**) Dose–response curves for purified recombinant PKCζ and PKCι kinase domains comparing CRT0066854, BIM-1 and Gö6983 chemical inhibitors. IC_{50} values are shown for the different inhibitors. The dots within the grey bar indicate the number and position of phosphorylation sites in different PKC isoenzymes used in the assay, confirmed by Western blots using site-specific anti-phospho-threonine antibodies. AL/TM/HM correspond to activation loop, turn motif and hydrophobic motif respectively. The precise phosphorylation site numbering for each PKC isoenzyme is given in Supplementary Table S1 at http://www.biochemj.org/bj/451/bj4510329add.htm. (**C**) CRT0066854 specifically inhibits aPKC in cells. Expression vectors encoding GFP–PKC isoforms were transfected into HCT-116 cells. Cells were treated in the presence or absence of CRT0066854 chemical inhibitor for the indicated time points before lysis. Cell lysates were immunoprecipitated with GFP–TRAP and immunoblotted (IB) with the indicated antibodies. Inhibitors were used at 10 μM (CRT0066854); 5 μM (Gö6983) and 10 μM (BIM-1) concentrations. (**D**) SPR analysis of binding of CRT0066854 to immobilized recombinant $PKC\iota_k$. Sensorgrams obtained for various CRT0066854 concentrations were flowed across the sensor chip (upper panel). RU, resonance units. Lower panel shows the steady-state binding isotherm of maximal response (RU_{max}) derived from fitting sensorgrams obtained over a range of CRT0066854 analyte concentrations to a one-site binding model. Affinity constant estimates from both methods are in close agreement.

Table 2 Effect of 1 μM CRT0066854 on the activity of 106 protein kinases

A radiometric assay was carried out by the Millipore Kinase Profiling Service (Millipore). The assay determined the selectivity of 1 μM single-point concentrations of CRT0066854 against a panel of 106 protein kinases and 30 μM ATP (K_m of PKCι_k). The selectivity score S(80) is the number of kinases inhibited by more than 80 % at 1 μM compound/total number of kinases tested. h, human; m, murine.

	Percentage of activity 1 μM CRT0066854	Percentage of inhibition 1 μM CRT0066854	
Abl(h)	93	11	1
Abl (M351T)(h)	97	3	2
ALK(h)	95	5	3
ARK5(h)	91	9	4
ASK1(h)	104	−4	5
Aurora-A(h)	96	−8	6
Axl(h)	106	−6	7
Blk(m)	98	2	8
Bmx(h)	107	−7	9
BRK(h)	112	−12	10
CDK1/cyclinB(h)	86	14	11
CDK2/cyclinA(h)	76	30	12
CDK5/p35(h)	32	68	13
CHK1(h)	100	0	14
CHK2(h)	90	10	15
CK1δ(h)	100	0	16
CK1γ1(h)	101	−1	17
CK1γ2(h)	120	−20	18
CK1γ3(h)	110	−10	19
cKit(h)	99	1	20
cKit(D816H)(h)	80	20	21
cKit(V560G)(h)	90	10	22
CSK(h)	103	−3	23
c-RAF(h)	94	3	24
cSRC(h)	89	8	25
DAPK1(h)	94	−3.5	26
DDR2(h)	108	−8	27
DYRK2(h)	94	6	28
EGFR(h)	102	−4	29
EGFR(L858R)(h)	78	22	30
EGFR(L861Q)(h)	87	13	31
EGFR(T790M)(h)	61	39	32
EGFR(T790M, L858R)(h)	69	31	33
EphA2(h)	102	−2	34
EphA7(h)	101	−1	35
EphB4(h)	106	−6	36
ErbB4(h)	102	−2	37
FAK(h)	99	1	38
Fer(h)	88	12	39
Fes(h)	91	9	40
FGFR1(h)	109	−9	41
FGFR2(h)	102	−2	42
FGFR3(h)	96	−11	43
FGFR4(h)	84	16	44
Flt1(h)	96	4	45
Flt3(D835Y)(h)	33	67	46
Flt3(h)	97	3	47
Flt4(h)	98	2	48
Fms(h)	96	4	49
GSK3α(h)	94	6	50
Hck(h)	92	8	51
HIPK1(h)	98	2	52
HIPK2(h)	93	7	53
HIPK3(h)	103	−3	54
IGF-1R(h)	88	12	55
IKKα(h)	29	65	56
IR(h)	85	15	57
IRAK4(h)	117	−17	58
JAK3(h)	94	6	59
JNK1α1(h)	102	−2	60
KDR(h)	96	4	61
LIMK1(h)	42	58	62
LKB1(h)	95	5	63
MAPKAP-K2(h)	101	−1	64
MAPK2(h)	99	1	65
MEK1(h)	100	−0.5	66
MELK(h)	77	23	67
Mer(h)	89	11	68
Met(h)	100	0	69
MSK1(h)	106	−6	70
MST1(h)	108	−8	71
MST3(h)	90	10	72
NEK2(h)	100	0	73
p70S6K(h)	88	12	74
PAK4(h)	103	−2	75
PDGFRα(h)	105	−5	76
PDGFRα(D842V)(h)	80	20	77
PDK1(h)	89	15	78
Pim-1(h)	89	11	79
PKBα(h)	96	−3.5	80
PKCα(h)	97	0	81
PKCβI(h)	107	−7	82
PKCγ(h)	102	−2	83
PKCδ(h)	89	11	84
PKCε(h)	99	−1	85
PKCη(h)	109	−5	86
PKCι(h)	13	83.5	87
PKCμ(h)	101	0	88
PKCθ(h)	108	−1	89
PKCζ(h)	23	77	90
PKD2(h)	96	4	91
Plk3(h)	83	17	92
PRK2(h)	16	84	93
Ret(h)	106	−6	94
ROCK-I(h)	109	−9	95
ROCK-II(h)	37	63	96
Ron(h)	114	−14	97
Ros(h)	94	6	98
SAPK2a(h)	102	−2	99
Snk(h)	102	−2	100
TAK1(h)	100	0	101
Tie2(h)	114	−14	102
TrkA(h)	114	−14	103
Yes(h)	102	−2	104
ZAP-70(h)	91	9	105
ZIPK(h)	86	14	106
			S(80)0.019

substituent including a benzyl group, a chiral carbon and a primary amine. The pyridine substituent acts as a kinase domain hinge-binding moiety by forming a hydrogen bond to the main-chain amide of Val[326], approximating to the position of the adenine ring of ATP. The primary amine of the 3-phenyl-propane-1,2-diamino headpiece of CRT0066854 makes a crucial charged interaction with both the backbone carbonyl of Asp[373] and the side chain of Asp[330]. Finally, the benzyl group in the inhibitor headpiece binds a small hydrophobic pocket formed by the kinase domain hinge, usually occupied by Phe[543] from the Ade motif [41] (Figure 2C; compare left-hand and middle panel). The benzyl group also makes an orthogonal π-stacking interaction with the pyridine ring hinge-binder, thus locking the inhibitor into a distinctly non-planar and U-shape conformation (Figure 2A).

Superimpositions of CRT0066854 and ATP-bound structures of PKCι_k indicate the general equivalence of the benzyl moiety and Phe[543] (Figure 2D). An important consequence of inhibitor binding is that the entire Ade motif, including Phe[543] from the Phe-Xaa-Xaa-Phe motif, becomes disordered, whereas it is an integral part of the ATP-binding cleft in the ATP–PKCι_k

Table 3 X-ray data collection and refinement statistics

Parameter	Values
Data collection	
Space group	$P3_1$
Cell dimensions	
a, *b*, *c* (Å)	113.6, 113.6, 82.4
α, β, γ (°)	90, 90, 120
Resolution (Å)*	49.2–2.74 (2.89–2.74)
R_{merge}	11.0 % (71.4 %)
R_{pim}	5.8 % (38.4 %)
I/σ	6.3 (1.1)
Completeness	100 % (100 %)
Multiplicity	5.6 (5.4)
Refinement	
Resolution (Å)	2.74
Number of unique reflections	31 307 (4570)
R_{work}/R_{free}	21.5 % / 25.6%
Atoms	
Protein	7468
Ligand/ion	180
Water	66
B-factors	
Protein	49.8
Ligand/ion	42.6
Water	31.9
RMSD	
Bond lengths (Å)	0.003
Bond angles (°)	0.726

*Numbers in parentheses are values in the highest resolution shell.

complex (PDB code 3A8W) (Figure 2C). Recent data have shown for PKCβ2, an equivalent phenyl side chain to Phe^{543} that has been implicated in allosteric activation [42]. This residue is held out of the ATP cleft by the C1 domain preventing full enzyme activation until diacylglycerol binds, providing an additional layer of PKC regulation. It seems likely that CRT0066854 targets PKCι_k for inhibition not only by competitive binding to the nucleotide-binding cleft, but also by preventing a catalytically competent conformation via displacement of the Ade motif by the benzyl inhibitor substituent. Both features combine to contribute towards the high specificity of CRT0066854 for aPKCs. A detailed comparison of inhibitor contents compared with other AGC kinases is given in the Supplementary Online Data and Supplementary Table S2 (at http://www.biochemj.org/bj/451/bj4510329add.htm).

CRT0066854 inhibition of LLGL2 phosphorylation in cells

LLGL is a recognized substrate of aPKC in *D. melanogaster* [43] and in immunocomplexes from HEK-293 cells expressing exogenous aPKC [44]. As LLGL2 is expressed at low levels in HEK-293 cells and due to the lack of a sensitive phospho-specific antibody against LLGL1/2, we used a co-expression system of aPKC and LLGL2 to evaluate the cellular IC_{50} of CRT0066854 in HEK-293 cells. Treatment of HEK-293 cells, co-transfected with PKCι wild-type and FLAG-tagged LLGL2, with CRT0066854 (0.125–8 μM) for 1 h led to a reproducible dose-dependent reduction in LLGL2 phosphorylation as seen by Western blotting (Figure 3A). In order to test this robustly in a high-throughput format, the phosphorylation signal window was optimized using the co-transfection of constitutively active PKCι-A120E [45] and FLAG-tagged LLGL2 and an ELISA was established. This demonstrated that CRT006854 has a cellular phospho-LLGL2 IC_{50} of 0.87 μM comparable with the IC_{50} measured *in vitro* against PKCι (Figure 3B).

Effect of CRT0066854 on A549 lung carcinoma cell viability

A549 cells are K-Ras mutant cells of lung origin, known to be dependent on PKCι for survival [17]. The A549 cells were treated with CRT0066854 for 48 h at various concentrations (0.01–20 μM), and cell viability determined by the CellTitre-Glo luminescent assay. An IC_{50} of 3.47 μM was obtained from three independent determinations (Figure 3C).

Decreased colony formation due to CRT0066854

Although a reduction in adherent cell growth has been reported following the depletion of PKCι in selected cell lines [46], the anti-proliferative effects appear more pronounced for non-adherent cell growth [17,46]. As such, we cultured HeLa cells, which reliably form colonies within 12 days when embedded in soft agar, and replenished inhibitor (0.1–10 μM) on alternate days. Two separate inhibitors were used for these experiments, the aPKC-specific CRT0066854 and its enantiomeric equivalent CRT0066390, which is essentially inactive towards PKCι *in vitro* (Table 1). At 1 μM the CRT0066854 inhibitor led to a 65 % decrease in colony formation and, as expected, the same dose of CRT0066390 resulted in considerably less suppression of colony formation (25 % decrease) (Figures 3D and 3E). This is consistent with CRT0066854 having a specific cellular effect via PKCι inhibition.

Inhibition of polarized epithelial morphogenesis by CRT0066854

Depletion of PKCι in cells using RNAi (RNA interference) leads to impaired luminal morphogenesis in epithelial cell 3D cysts as a consequence of impaired spindle formation and apical–basal polarity [9,47]. We therefore tested whether chemical inhibition could induce the same phenotype in MDCK cells embedded in Matrigel™. MDCK cells are widely used as models for studying epithelia, as they have clear apical–basolateral polarity and polarize in 2D (two-dimensional) and 3D cell cultures. In Matrigel™, MDCK cells are known to form cysts with a single lumen. We determined the number of MDCK cysts that had a PSAL (predominantly single apical lumen) after growing in the presence of 0, 0.33 or 1 μM concentrations of CRT0066854. Surprisingly, inhibitor addition caused significant disruption to lumen formation, resulting in a multiple luminal morphology (Figure 4A). This disruption in lumen formation was dose-dependent and quantification of this effect indicated that at 1 μM concentrations of CRT0066854 there was a 50 % reduction in PSALs compared with a DMSO control (Figure 4B).

CRT0066854 impedes directed migration of NRK cells

Depletion of aPKC using RNAi decreases the rate of healing in an NRK cell scratch-wound assay due to an impairment of the polarized delivery of the exocyst to the cell's leading edge [10]. We used this model to test the effect of aPKC inhibition by CRT0066854 on directional migration. Scratch wounds were generated in wells of confluent NRK cells after which DMSO, or 3, 6 or 12 μM CRT0066854 was added to the wells and time-lapse imaging recorded the wound healing over 10 h (Supplementary Movie S1 at http://www.biochemj.org/bj/451/bj4510329add.htm). Both 6 μM and 12 μM CRT0066854 led to a significant reduction in wound healing, with 12 μM halving the normalized migration speed (Figures 4C and 4D). Note that optimum knockdown of aPKCs in this model reduces migration by 60 % [10].

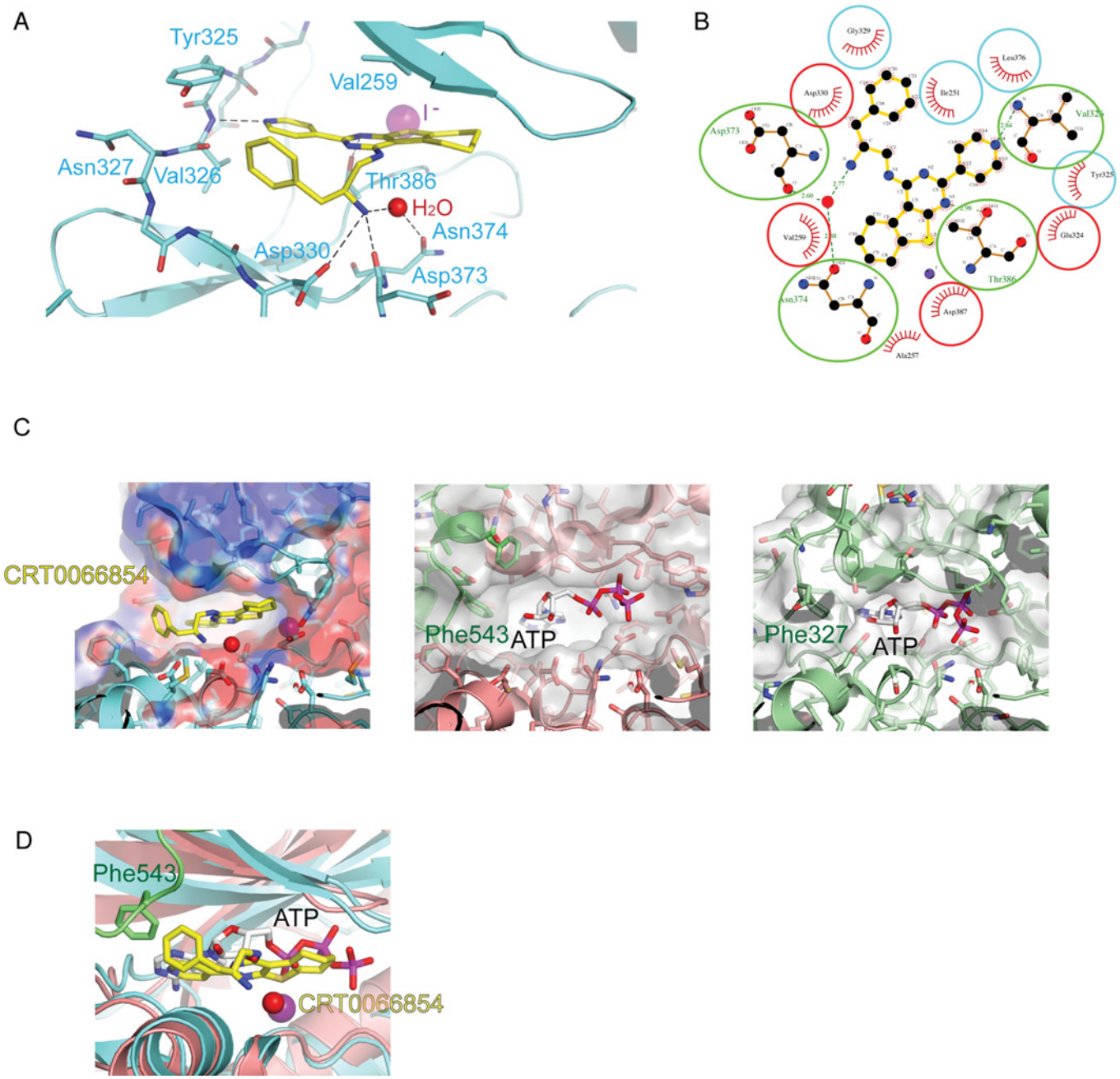

Figure 2 Structural basis for CRT0066854 inhibition of PKCι_k

(**A**) Close-up of the CRT0066854-binding site within the PKCι nucleotide-binding cleft and kinase domain hinge, highlighting the five hydrogen-bond contacts and the lack of planarity of CRT0066854. Selected protein side chains and main chains are shown for clarity. A bound water molecule (red sphere) and an iodide ion (purple sphere) are also shown. (**B**) A 2D representation of CRT0066854 inhibitor–PKCι contacts produced by LIGPLOT + [51]. (**C**) Comparison of the nucleotide pockets between CRT0066854 and ATP complexes of PKCι. The left-hand panel shows the electrostatic surface of PKCι, including the two acidic residues that interact with the inhibitor (yellow sticks). Phe^{543} from the Asn-Phe-Asp motif of PKCι (middle panel, green sticks and salmon-pink cartoon) contacts ATP in a similar manner to Phe^{327} of protein kinase A (right-hand panel, green cartoon and sticks). Inhibitor binding leads to (i) displacement of the Asn-Phe-Asp motif (left-hand panel), (ii) changes in the glycine loop, and (iii) changes in the Tyr^{256} (glycine loop)–Trp^{289} (Cα-helix) interaction. (**D**) Superimposition of the nucleotide-binding pockets of PKCι bound to ATP and to CRT0066854. This shows that the phenyl group of CRT0066854 (yellow sticks) mimics the placement of Phe^{543} (green sticks) from the Ade motif observed in the ATP complex.

DISCUSSION

In the present study, we report the identification and characterization of a selective inhibitor of the aPKC isoenzymes. Selectivity and potency issues have proved particularly challenging in the search for inhibitors of individual PKC isoforms, particularly aPKCζ and aPKCι, where all commercially available inhibitors have greater efficacy for the cPKCs and nPKCs [34]. The discovery of CRT0066854 and a knowledge of the detailed contacts it makes within the aPKC kinase ATP-binding cleft demonstrates that isoform specificity can be obtained using the residues surrounding the nucleotide-binding site, and provides a useful starting point for rational design of even more potent and specific inhibitors.

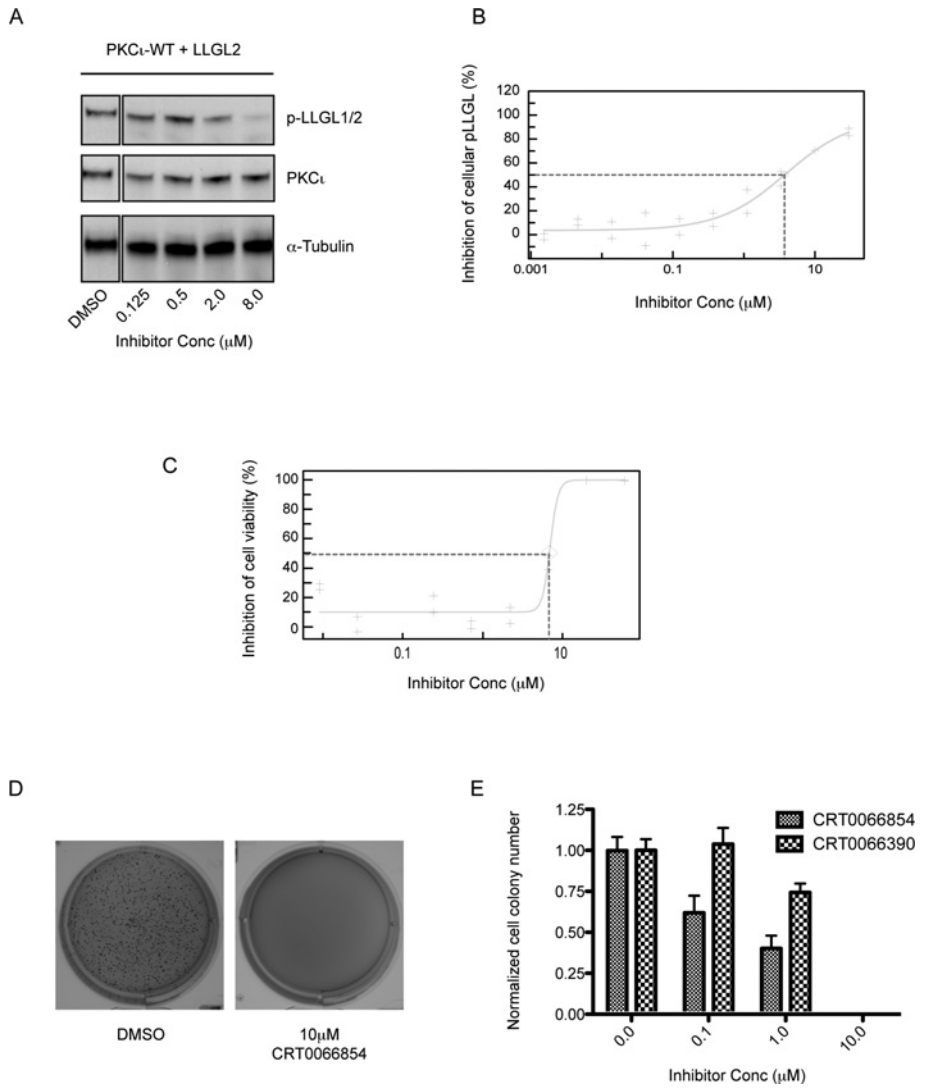

Figure 3 CRT0066854 inhibits LLGL2 phosphorylation and cell viability

(**A**) HEK-293 cells were co-transfected with LLGL2 and PKCι-WT (wild-type). After 35 h, the cells were treated with CRT0066854 (0.125–8 μM) for 1 h, lysates were generated separated by gel electrophoresis and immunoblotted with pLLGL1/2. (**B**) HEK-293 cells co-transfected with FLAG–LLGL2 and PKCι-A120E (constitutively active). After 40 h, cells were treated with CRT0066854 (0.001–12 μM) for 1 h and an ELISA was performed. (**C**) A549 cells in log-phase growth as a monolayer were treated with CRT0066854 at the indicated concentrations for 48 h and the cell viability was estimated using CellTitreGlo. (**D**) HeLa cells from a single cell suspension were cultured in soft agar for 14 days, with the medium and inhibitor being replenished on alternate days. Colonies were stained with Crystal Violet and images of the 35-mm well taken using a mounted CCD camera. (**E**) The effect of aPKC inhibitors on HeLa colony growth was quantified and the means $\pm$ S.E.M. is presented for at least three separate experiments.

Our crystallographic analysis has revealed that CRT0066854 has a bifunctional inhibitory effect. First, it is a competitive ATP inhibitor, binding within the nucleotide-binding pocket of aPKC. Secondly, it uses a benzyl group to displace the Ade motif from a peripheral hinge pocket adjacent to the nucleotide cleft and prevents it forming a functional ATP-binding pocket. These two features ensure that CRT0066854 is highly selective for aPKC. Some strain/induced fit is evident within the compound in view of its lack of planarity when bound to PKCι_k. Inhibitory effects on other kinases such as ROCK2 and PRK2 may be due to the presence of a similar phenyl group equivalent to Phe^{543}, suggesting that related scaffolds may permit a more generic approach towards inhibiting AGC kinases bearing an Asn-Phe-Asp motif. Binding isotherms show that the inhibitor has a low off-rate, generally deemed to be an advantageous feature for a kinase inhibitor.

Recent studies have shown differential effects between PKCζ and PKCι for compounds targeting other aPKC-specific pockets outside of the ATP cleft [35,48]. The selectivity of CRT0066854 shown in the present study for both aPKCζ and aPKCι could prove useful in both clinical and research settings. We provide compelling evidence for both *in vitro* and phenotypic effects of CRT0066854 using a range of cellular assays relevant to cancer therapy. Non-adherent cell growth, migration and aberrant polarity are all processes exploited by cancer and were more affected by CRT0066854 than adherent cell growth. This differential dependence on aPKC for 3D and 2D cellular phenotypes has been demonstrated previously by genetic depletion of aPKC [17], and together with the work described in the present paper, supports the role of CRT0066854 as a selective aPKC inhibitor in cells. PKCι overexpression has been linked to

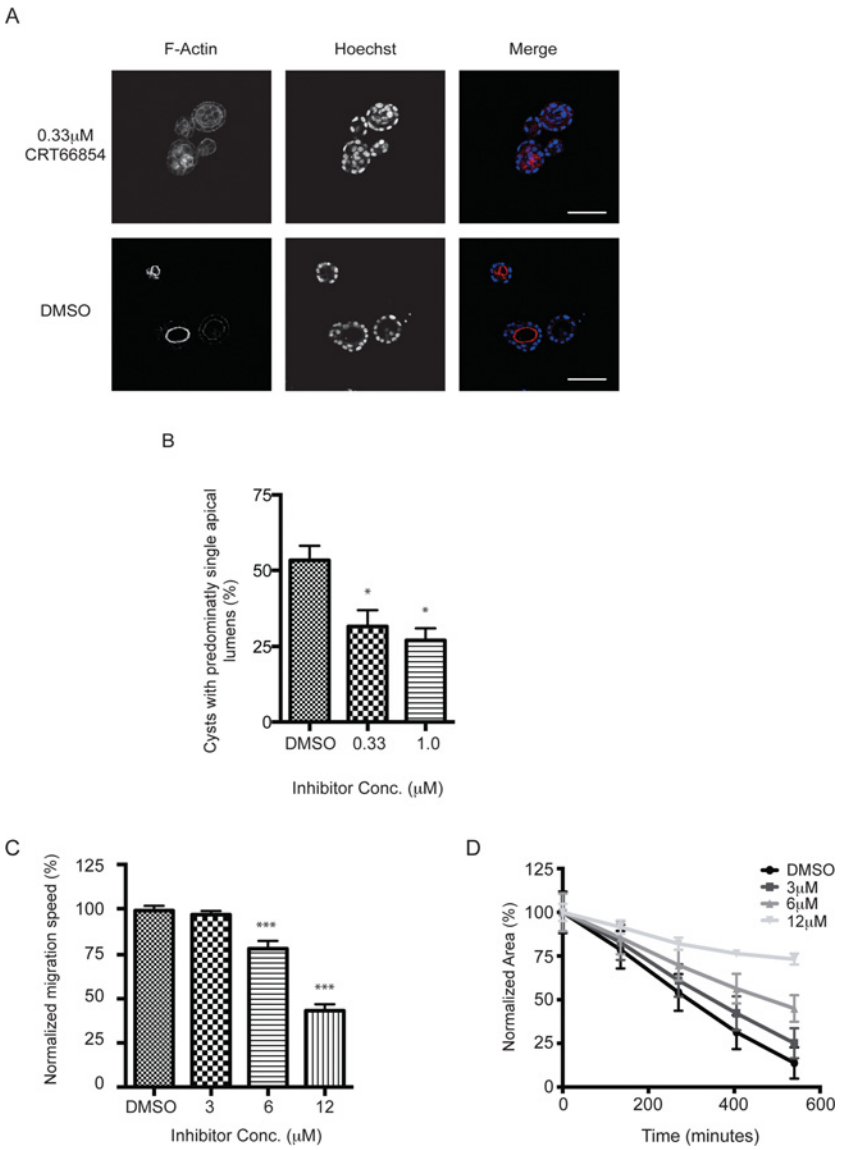

Figure 4 Phenotypic effects of CRT0066854 on cell polarity and directed cell migration

(**A**) MDCK cells were cultured in Matrigel™ for 6 days. The cultures were treated with 0, 0.33 or 1 μM of the aPKCι inhibitor CRT0066854 which were replenished, along with growth medium, on alternate days. Cultures were fixed and stained with Phalloidin (F-actin) and counterstained with Hoechst (DNA). Representative single mid-section confocal images are shown. The scale bars represent 50 μM. (**B**) Quantification of the number of PSALs was made. At least 100 cysts were counted per condition in each experiment and the means $\pm$ S.E.M. are presented for at least three separate experiments. (**C**) Confluent monolayers of NRK cells were wounded, treated with CRT0066854 at the indicated concentrations and healing was followed over time. The panels shown are representative of at least three independent experiments. (**D**) The normalized mean migration speed is plotted for different CRT0066854 concentrations. The error bars represent the S.E.M. and one-way ANOVA was used to determine statistical significance of difference: $^{*}P < 0.05$, $^{***}P < 0.001$.

several types of cancer, including non-small-cell lung cancer and ovarian cancer [17,49,50] and further optimization of inhibitors on the basis of the CRT0066854 structure could yield more specific cancer therapeutics. CRT0066854 and its derivative compounds will be useful tools to further dissect PKCζ and PKCι roles in establishing cell polarity and growth-factor-stimulated signalling pathways.

AUTHOR CONTRIBUTION

Svend Kjær purified, assembled and crystallized the CRT0066854 inhibitor–PKCι_k complex; Andrew Purkiss collected the data, and determined and refined the CRT0066854-bound structure; Brenda Kostelecky and Erika Soriano carried out kinetic assays with inhibitors; Phillip Knowles carried out the SPR experiments; Philippe Riou assessed inhibitor efficacy against multiple PKC isoforms in cells; Christian Dillon and Jon Roffey led the chemistry project team that discovered CRT0066854; Caroline Barton and Bhavisha Patel conducted the LLGL2 phosphorylation assays and cell viability assay; Christelle Soudy synthesized the inhibitors used in these studies; Carine Rosse conducted the directed cell migration assay; Sarah Kaye carried out IC_{50} assays on full-length aPKC isoenzymes; Mark Linch carried out the LLGL2 phosphorylation assay, cell polarity and colony formation assay; Peter Parker and Neil McDonald planned the project and designed experiments; and Neil McDonald, Judith Murray-Rust and Mark Linch prepared the Figures and wrote the paper.

ACKNOWLEDGEMENTS

We thank members of the N.Q.M. and P.J.P. laboratories for helpful discussions and comments on the paper before submission. We gratefully acknowledge the expert assistance of Tamar Telem-Shafir (GE Healthcare) in performing and analysing the SPR data.

FUNDING

S. Kjær was funded by a Cancer Research UK fellowship and by a Marie Curie Fellowship [grant number MEIF-CT-2005-010656]; M.L. was funded by a Cancer Research UK Clinical Research Fellowship. Research in the N.Q.M. and P.J.P. laboratories is supported by CRUK core funding to the London Research Institute.

REFERENCES

1 Bosco, R., Melloni, E., Celeghini, C., Rimondi, E., Vaccarezza, M. and Zauli, G. (2011) Fine tuning of protein kinase C (PKC) isoforms in cancer: shortening the distance from the laboratory to the bedside. Mini-Rev. Med. Chem. **11**, 185–199
2 Rosse, C., Linch, M., Kermorgant, S., Cameron, A. J., Boeckeler, K. and Parker, P. J. (2010) PKC and the control of localized signal dynamics. Nat. Rev. Mol. Cell Biol. **11**, 103–112
3 Parker, P. J. and Murray-Rust, J. (2004) PKC at a glance. J. Cell Sci. **117**, 131–132
4 Pearce, L. R., Komander, D. and Alessi, D. R. (2010) The nuts and bolts of AGC protein kinases. Nat. Rev. Mol. Cell Biol. **11**, 9–22
5 Suzuki, A., Akimoto, K. and Ohno, S. (2003) Protein kinase C λ/ι (PKCλ/ι): a PKC isotype essential for the development of multicellular organisms. J. Biochem. **133**, 9–16
6 Knoblich, J. A. (2010) Asymmetric cell division: recent developments and their implications for tumour biology. Nat. Rev. Mol. Cell Biol. **11**, 849–860
7 Suzuki, A. and Ohno, S. (2006) The PAR–aPKC system: lessons in polarity. J. Cell Sci. **119**, 979–987
8 Hao, Y., Du, Q., Chen, X., Zheng, Z., Balsbaugh, J. L., Maitra, S., Shabanowitz, J., Hunt, D. F. and Macara, I. G. (2010) Par3 controls epithelial spindle orientation by aPKC-mediated phosphorylation of apical Pins. Curr. Biol. **20**, 1809–1818
9 Durgan, J., Kaji, N., Jin, D. and Hall, A. (2011) Par6B and atypical PKC regulate mitotic spindle orientation during epithelial morphogenesis. J. Biol. Chem. **286**, 12461–12474
10 Rosse, C., Formstecher, E., Boeckeler, K., Zhao, Y., Kremerskothen, J., White, M. D., Camonis, J. H. and Parker, P. J. (2009) An aPKC–exocyst complex controls paxillin phosphorylation and migration through localised JNK1 activation. PLoS Biol. **7**, e1000235
11 Etienne-Manneville, S. and Hall, A. (2003) Cell polarity: Par6, aPKC and cytoskeletal crosstalk. Curr. Opin. Cell Biol. **15**, 67–72
12 Fields, A. P. and Regala, R. P. (2007) Protein kinase C iota: human oncogene, prognostic marker and therapeutic target. Pharmacol. Res. **55**, 487–497
13 Guo, H., Gu, F., Li, W., Zhang, B., Niu, R., Fu, L., Zhang, N. and Ma, Y. (2009) Reduction of protein kinase C ζ inhibits migration and invasion of human glioblastoma cells. J. Neurochem. **109**, 203–213
14 Liu, Y., Wang, B., Wang, J., Wan, W., Sun, R., Zhao, Y. and Zhang, N. (2009) Down-regulation of PKCζ expression inhibits chemotaxis signal transduction in human lung cancer cells. Lung Cancer **63**, 210–218
15 Sun, R., Gao, P., Chen, L., Ma, D., Wang, J., Oppenheim, J. J. and Zhang, N. (2005) Protein kinase C ζ is required for epidermal growth factor-induced chemotaxis of human breast cancer cells. Cancer Res. **65**, 1433–1441
16 Xu, L. and Deng, X. (2006) Protein kinase Cι promotes nicotine-induced migration and invasion of cancer cells via phosphorylation of μ- and m-calpains. J. Biol. Chem. **281**, 4457–4466
17 Regala, R. P., Weems, C., Jamieson, L., Copland, J. A., Thompson, E. A. and Fields, A. P. (2005) Atypical protein kinase Cι plays a critical role in human lung cancer cell growth and tumorigenicity. J. Biol. Chem. **280**, 31109–31115
18 Aranda, V., Haire, T., Nolan, M. E., Calarco, J. P., Rosenberg, A. Z., Fawcett, J. P., Pawson, T. and Muthuswamy, S. K. (2006) Par6-aPKC uncouples ErbB2 induced disruption of polarized epithelial organization from proliferation control. Nat. Cell Biol. **8**, 1235–1245
19 Brumby, A. M. and Richardson, H. E. (2003) *scribble* mutants cooperate with oncogenic Ras or Notch to cause neoplastic overgrowth in *Drosophila*. EMBO J. **22**, 5769–5779
20 Pagliarini, R. A. and Xu, T. (2003) A genetic screen in *Drosophila* for metastatic behavior. Science **302**, 1227–1231
21 Duran, A., Linares, J. F., Galvez, A. S., Wikenheiser, K., Flores, J. M., Diaz-Meco, M. T. and Moscat, J. (2008) The signaling adaptor p62 is an important NF-κB mediator in tumorigenesis. Cancer Cell **13**, 343–354
22 Regala, R. P., Davis, R. K., Kunz, A., Khoor, A., Leitges, M. and Fields, A. P. (2009) Atypical protein kinase C ι is required for bronchioalveolar stem cell expansion and lung tumorigenesis. Cancer Res. **69**, 7603–7611
23 Yang, Y. L., Chu, J. Y., Luo, M. L., Wu, Y. P., Zhang, Y., Feng, Y. B., Shi, Z. Z., Xu, X., Han, Y. L., Cai, Y. et al. (2008) Amplification of PRKCI, located in 3q26, is associated with lymph node metastasis in esophageal squamous cell carcinoma. Genes, Chromosomes Cancer **47**, 127–136
24 Kojima, Y., Akimoto, K., Nagashima, Y., Ishiguro, H., Shirai, S., Chishima, T., Ichikawa, Y., Ishikawa, T., Sasaki, T., Kubota, Y. et al. (2008) The overexpression and altered localization of the atypical protein kinase C λ/ι in breast cancer correlates with the pathologic type of these tumors. Hum. Pathol. **39**, 824–831
25 Scotti, M. L., Bamlet, W. R., Smyrk, T. C., Fields, A. P. and Murray, N. R. (2010) Protein kinase Cι is required for pancreatic cancer cell transformed growth and tumorigenesis. Cancer Res. **70**, 2064–2074
26 Takagawa, R., Akimoto, K., Ichikawa, Y., Akiyama, H., Kojima, Y., Ishiguro, H., Inayama, Y., Aoki, I., Kunisaki, C., Endo, I. et al. (2010) High expression of atypical protein kinase C λ/ι in gastric cancer as a prognostic factor for recurrence. Ann. Surg. Oncol. **17**, 81–88
27 Li, Q., Wang, J. M., Liu, C., Xiao, B. L., Lu, J. X. and Zou, S. Q. (2008) Correlation of aPKC-ι and E-cadherin expression with invasion and prognosis of cholangiocarcinoma. Hepatobiliary Pancreatic Dis. Int. **7**, 70–75
28 Patel, R., Win, H., Desai, S., Patel, K., Matthews, J. A. and Acevedo-Duncan, M. (2008) Involvement of PKC-ι in glioma proliferation. Cell Proliferation **41**, 122–135
29 Murray, N. R. and Fields, A. P. (1997) Atypical protein kinase C ι protects human leukemia cells against drug-induced apoptosis. J. Biol. Chem. **272**, 27521–27524
30 Baldwin, R. M., Garratt-Lalonde, M., Parolin, D. A., Krzyzanowski, P. M., Andrade, M. A. and Lorimer, I. A. (2006) Protection of glioblastoma cells from cisplatin cytotoxicity via protein kinase Cι -mediated attenuation of p38 MAP kinase signaling. Oncogene **25**, 2909–2919
31 Jin, Y. T., Ying, X. X., Hu, Y. H., Zou, Q., Wang, H. Y. and Xu, Y. H. (2008) aPKC inhibitors might be the sensitizer of chemotherapy and adoptive immunotherapy in the treatment of hASIPa-overexpressed breast cancer. Oncol. Res. **17**, 59–68
32 Kikuchi, K., Soundararajan, A., Zarzabal, L. A., Weems, C. R., Nelon, L. D., Hampton, S. T., Michalek, J. E., Rubin, B. P., Fields, A. P. and Keller, C. (2012) Protein kinase C ι as a therapeutic target in alveolar rhabdomyosarcoma. Oncogene **32**, 286–95
33 Knight, Z. A. and Shokat, K. M. (2005) Features of selective kinase inhibitors. Chem. Biol. **12**, 621–637
34 Roffey, J., Rosse, C., Linch, M., Hibbert, A., McDonald, N. Q. and Parker, P. J. (2009) Protein kinase C intervention: the state of play. Curr. Opin. Cell Biol. **21**, 268–279
35 Frohner, W., Lopez-Garcia, L. A., Neimanis, S., Weber, N., Navratil, J., Maurer, F., Stroba, A., Zhang, H., Biondi, R. M. and Engel, M. (2011) 4-Benzimidazolyl-3-phenylbutanoic acids as novel PIF-pocket-targeting allosteric inhibitors of protein kinase PKCζ. J. Med. Chem. **54**, 6714–6723
36 Erdogan, E., Lamark, T., Stallings-Mann, M., Lee, J., Pellecchia, M., Thompson, E. A., Johansen, T. and Fields, A. P. (2006) Aurothiomalate inhibits transformed growth by targeting the PB1 domain of protein kinase Cι. J. Biol. Chem. **281**, 28450–28459
37 Collaborative Computational Project-Number 4 (1994) The CCP-4 suite: programs for protein crystallography. Acta Crystallogr., Sect. D: Biol. Crystallogr. **50**, 760–763
38 McCoy, A. J., Grosse-Kunstleve, R. W., Adams, P. D., Winn, M. D., Storoni, L. C. and Read, R. J. (2007) Phaser crystallographic software. J. Appl. Crystallogr. **40**, 658–674
39 Adams, P. D., Grosse-Kunstleve, R. W., Hung, L. W., Ioerger, T. R., McCoy, A. J., Moriarty, N. W., Read, R. J., Sacchettini, J. C., Sauter, N. K. and Terwilliger, T. C. (2002) PHENIX: building new software for automated crystallographic structure determination. Acta Crystallogr., Sect. D: Biol. Crystallogr. **58**, 1948–1954
40 Bain, J., Plater, L., Elliott, M., Shpiro, N., Hastie, C. J., McLauchlan, H., Klevernic, I., Arthur, J. S., Alessi, D. R. and Cohen, P. (2007) The selectivity of protein kinase inhibitors: a further update. Biochem. J. **408**, 297–315
41 Romano, R. A., Kannan, N., Kornev, A. P., Allison, C. J. and Taylor, S. S. (2009) A chimeric mechanism for polyvalent trans-phosphorylation of PKA by PDK1. Protein Sci. **18**, 1486–1497
42 Leonard, T. A., Rozycki, B., Saidi, L. F., Hummer, G. and Hurley, J. H. (2011) Crystal structure and allosteric activation of protein kinase C βII. Cell **144**, 55–66
43 Betschinger, J., Mechtler, K. and Knoblich, J. A. (2003) The Par complex directs asymmetric cell division by phosphorylating the cytoskeletal protein Lgl. Nature **422**, 326–330
44 Plant, P. J., Fawcett, J. P., Lin, D. C., Holdorf, A. D., Binns, K., Kulkarni, S. and Pawson, T. (2003) A polarity complex of mPar-6 and atypical PKC binds, phosphorylates and regulates mammalian Lgl. Nat. Cell Biol. **5**, 301–308
45 Pears, C. J., Kour, G., House, C., Kemp, B. E. and Parker, P. J. (1990) Mutagenesis of the pseudosubstrate site of protein kinase C leads to activation. Eur. J. Biochem. **194**, 89–94
46 Ishiguro, H., Akimoto, K., Nagashima, Y., Kojima, Y., Sasaki, T., Ishiguro-Imagawa, Y., Nakaigawa, N., Ohno, S., Kubota, Y. and Uemura, H. (2009) aPKCλ/ι promotes growth of prostate cancer cells in an autocrine manner through transcriptional activation of interleukin-6. Proc. Natl. Acad. Sci. U.S.A. **106**, 16369–16374
47 Horikoshi, Y., Suzuki, A., Yamanaka, T., Sasaki, K., Mizuno, K., Sawada, H., Yonemura, S. and Ohno, S. (2009) Interaction between PAR-3 and the aPKC–PAR-6 complex is indispensable for apical domain development of epithelial cells. J. Cell Sci. **122**, 1595–1606

48 Pillai, P., Desai, S., Patel, R., Sajan, M., Farese, R., Ostrov, D. and Acevedo-Duncan, M. (2011) A novel PKC-ι inhibitor abrogates cell proliferation and induces apoptosis in neuroblastoma. Int. J. Biochem. Cell Biol. **43**, 784–794
49 Eder, A. M., Sui, X., Rosen, D. G., Nolden, L. K., Cheng, K. W., Lahad, J. P., Kango-Singh, M., Lu, K. H., Warneke, C. L., Atkinson, E. N. et al. (2005) Atypical PKCι contributes to poor prognosis through loss of apical-basal polarity and cyclin E overexpression in ovarian cancer. Proc. Natl. Acad. Sci. U.S.A. **102**, 12519–12524
50 Zhang, L., Huang, J., Yang, N., Liang, S., Barchetti, A., Giannakakis, A., Cadungog, M. G., O'Brien-Jenkins, A., Massobrio, M., Roby, K. F. et al. (2006) Integrative genomic analysis of protein kinase C (PKC) family identifies PKCι as a biomarker and potential oncogene in ovarian carcinoma. Cancer Res. **66**, 4627–4635
51 Laskowski, R. A. and Swindells, M. B. (2011) LigPlot + : multiple ligand–protein interaction diagrams for drug discovery. J. Chem. Inf. Model. **51**, 2778–2786

Received 18 December 2012/12 February 2013; accepted 18 February 2013
Published as BJ Immediate Publication 18 February 2013, doi:10.1042/BJ20121871

Biochem. J. (2013) **451**, 329–342 (Printed in Great Britain) doi:10.1042/BJ20121871

multimedia online data

SUPPLEMENTARY ONLINE DATA

Adenosine-binding motif mimicry and cellular effects of a thieno[2,3-*d*]pyrimidine-based chemical inhibitor of atypical protein kinase C isoenzymes

Svend KJÆR*[1], Mark LINCH†[1], Andrew PURKISS*, Brenda KOSTELECKY*†, Phillip P. KNOWLES*, Carine ROSSE†, Philippe RIOU†, Christelle SOUDY‡, Sarah KAYE‡, Bhavisha PATEL‡, Erika SORIANO*, Judith MURRAY-RUST*, Caroline BARTON‡, Christian DILLON‡, Jon ROFFEY‡, Peter J. PARKER†§[2] and Neil Q. McDONALD*‖[2]

*Structural Biology, Cancer Research UK, 44 Lincoln's Inn Fields, London WC2A 3LY, U.K., †Protein Phosphorylation Laboratories, Cancer Research UK, 44 Lincoln's Inn Fields, London WC2A 3LY, U.K., ‡Cancer Research Technology Discovery Laboratories, Wolfson Institute for Biomedical Research, University College London, Gower Street, London WC1E 6BT, U.K., §Division of Cancer Studies, King's College London, New Hunts House, Guy's Campus, London SE1 1UL, U.K., and ‖Institute of Structural and Molecular Biology, Department of Biological Sciences, Birkbeck College, University of London, Malet Street, London WC1E 7HX, U.K.

CRT0066854-bound PKCι_k adopts an active kinase conformation

Both PKCι_k structures bound to ATP (PDB code 3A8W) or bound to CRT0066854, have similar relative N-lobe and C-lobe orientations consistent with a closed 'active' kinase conformation. Active kinase conformational elements include (i) an occupied nucleotide-binding pocket, (ii) an ordered activation loop and (iii) a salt bridge between the Cα-helix Glu^{293} and N-lobe Lys^{274} that co-ordinates ATP phosphate moieties adjacent to the predicted divalent metal site. The glycine-rich loop of PKCι_k bound to CRT0066854 adopts a 'closed' conformation making multiple van der Waals contacts with the inhibitor (Figure 2 in the main text). The threonine residues of the activation loop (Thr^{403}) and the turn motif (Thr^{555}) are phosphorylated in both PKCι_k structures. Comparison with other PKC kinase domain structures shows considerable variation in the precise position of the turn motif, indicating some plasticity within this poorly conserved region. The hydrophobic motif (residues 570–578) is well ordered and are bound to the hydrophobic cleft of the N-lobe as expected.

Structural comparisons of CRT0066854 and BIM-1 bound to the PKCι kinase domain

We compared contact residues from the CRT0066854 and BIM-1 complexes to further characterize the selectivity of the aPKC-selective inhibitor. This analysis does not consider the contribution of bound solvent between inhibitor and protein as few ordered solvent molecules are observed for these structures given their modest resolution. Supplementary Table S2 shows the contact residues together with their structural equivalents in other classes of PKC isoenzymes, the AGC kinases PKA (protein kinase A), PKB (protein kinase B) as well as PRK2 and ROCK (both inhibited by CRT0066854, Table 2 in the main text). Of the PKCι side chains involved in CRT0066854 binding, BIM-1 binding or both, five residues stand out: Ile^{251}, Val^{307}, Ile^{323}, Leu^{376} and Thr^{386} (Figure 2B of the main text). Thr^{386} is a good candidate for conferring CRT0066854 sensitivity on aPKCs owing to its side-chain hydrogen bond to a nitrogen atom of the thieno[2,3-*d*]pyrimidine scaffold of CRT0066854. The equivalent residue in most other PKC isoforms is alanine, which is unable to form such a side-chain hydrogen bond. ROCK2 and PRK2 also have alanine at this position. The exception is PKCγ, which also contains threonine at this position, as do PKB and PKA. However, PKB and PKCγ are unresponsive to CRT0066854 at 1 μM inhibitor concentration in *in vitro* assays, compared with 77 % inhibition for PKCζ (Table 2 in the main text).

Both aPKCs and nPKCs have a leucine residue at position 376, whereas cPKCs have methionine. The higher potency of BIM-1 towards cPKC isoenzymes may be influenced by a methionine residue at this position as has been suggested for PKB [1]. However, the presence of Leu^{376} alone cannot account for CRT0066854 potency towards aPKC over nPKCs. Val^{307} of aPKCs aligns with threonine in the cPKC and nPKC isoforms as well as in PKB. The side-chain oxygen of this threonine residue is involved in binding BIM-1, whereas such an equivalent interaction is not possible for the aPKC isoenzymes. Val^{307} may thus select against BIM-1 binding [2]. The equivalent to the gatekeeper residue Ile^{323} is methionine in all cPKC and nPKC isoforms as well as in PKB, PKA, PRK2 and ROCK2. The Ile^{323} side chain forms hydrophobic contacts with CRT0066854 and, although the hydrophobic methionine would add some additional bulk, its presence in PRK2 and ROCK2 suggests that it does not perturb CRT0066854 binding. Ile^{251} may also play a role in drug selectivity. Isoleucine at this position is unique to the aPKCs, and ROCK2 with the equivalent residue being leucine in all other PKCs and many AGC kinases. The slight change induced by the isoleucine to leucine switch may also help to determine the difference in BIM-1 sensitivities for the respective isoforms. The AGC kinases PRK2 and ROCK2 are both inhibited to a significant extent by CRT0066854. Each has an Asn-Phe-Asp motif and therefore may provide a positive selection for these kinases to bind CRT0066854 in a similar manner to PKCι. We conclude that rather than depending on a single individual side chain, a combination of several residues is responsible for the isoform specificity of CRT0066854 for aPKCs by both selecting for this inhibitor, as well as selecting against CRT0066854 in other AGC kinases.

[1] These authors contributed equally to this work.

[2] Correspondence may be addressed to either of these authors (email neil.mcdonald@cancer.org.uk or peter.parker@cancer.org.uk).

The structural co-ordinates for PKCι_k bound to CRT0066854 will appear in the PDB under the accession number 3ZH8.

Table S1 Selected PKC kinase domain kinetic constants

AL/TM/HM, activation loop, turn motif and hydrophobic motif. Values are presented as means±S.E.M.

Kinase domain phosphorylation	k_{cat} (min^{-1})	K_m (μM)
PKCε_k AL/TM/HM (pT566/pT710/pS729)	147.6±4.8	28.8±2.8
PKCι_k AL/TM/HM* (pT403/pT555/E574)	199.0±3.3	65.4±2.6
PKCζ_k AL/TM/HM* (pT410/pT560/E579)	178.6±1.6	25.9±0.7

*The HM phospho-acceptor is a glutamate residue.

Table S2 Inhibitor contacts with residues within the PKCι_k nucleotide-binding cleft and comparisons with other AGC kinases

Structurally equivalent residues contacting inhibitors in the nucleotide-binding sites of PKCι, PKCβII (a cPKC) and a nPKC are shown. Also included are the equivalent residues in four other AGC kinases, two of which (ROCK2 and PRK2) are also inhibited by CRT0066854 (see Table 2 in the main text). Residues in bold indicate the residue was involved in binding the inhibitor indicated in the row header. Residues in italics indicate the equivalent residues to those shown in bold for the indicated proteins. Asterisks indicate functional residues conserved in all kinases. Underlined residues indicate those residues proposed to be important for BIM-1 and CRT0066854 binding specificity. PKA, protein kinase A; PKB, protein kinase B.

PKCι CRT0066854	PKCι BIM-1	PKCβII miBIM-1	nPKC	ROCK2	PRK2	PKA	PKB
Ile^{251}	**Ile^{251}**	**Leu^{348}**	**Leu**	Ile	Leu	Leu	Leu
*Gly^{252}**	**Gly^{252}**	**Gly^{349}**	**Gly**	Gly	Gly	Gly	Gly
Gly^{254}*	*Gly^{254}*	*Gly^{351}*	*Gly*	Gly	Gly	Gly	Gly
Val^{259}	**Val^{259}**	**Val^{356}**	**Val**	Val	Val	Val	Val
Ala^{272}	**Ala^{272}**	**Ala^{369}**	**Ala**	Ala	Ala	Ala	Ala
Lys^{274}*	**Lys^{274}**	*Lys^{371}*	*Lys*	Lys	Lys	Lys	Lys
Val^{307}	*Val^{307}*	**Thr^{404}**	**Thr**	Val	Val	Val	Thr
Ile^{323}	*Ile^{323}*	*Met^{420}*	*Met*	Met	Met	Met	Met
Tyr^{325}	*Tyr^{325}*	*Tyr^{422}*	*Tyr/Phe*	Tyr	Tyr	Tyr	Tyr
Val^{326}	**Val^{326}**	**Val^{423}**	**Val**	Met	Ala	Val	Ala
Gly^{329}	*Gly^{329}*	*Gly^{426}*	*Gly*	Gly	Gly	Gly	Gly
Asp^{330}	*Asp^{330}*	*Asp^{427}*	*Asp*	Asp	Asp	Glu	Glu
Asp^{373}	**Asp^{373}**	*Asp^{470}*	*Asp*	Asp	Asp	Glu	Glu
Leu^{376}	**Leu^{376}**	**Met^{473}**	Leu	Leu	Leu	Leu	Met
Thr^{386}	**Thr^{386}**	**Ala^{483}**	**Ala**	Ala	Ala	Thr	Thr
Asp^{387}*	**Asp^{387}**	**Asp^{484}**	**Thr**	Asp	Asp	Asp	Asp

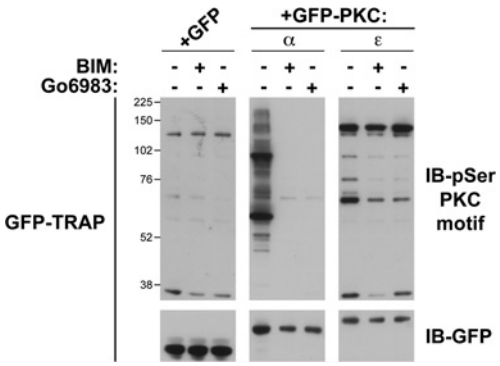

Figure S1 Inhibition of cPKCs and nPKCs in cells by use of cPKC inhibitors can be detected biochemically

Expression vectors encoding GFP–PKC isoforms were transfected into HCT-116 cells. Cells were treated with chemical inhibitors (BIM-1 and Gö6983) for 2 h before lysis. Cell lysates were immunoprecipitated with GFP–TRAP and immunoblotted (IB) with the indicated antibodies.

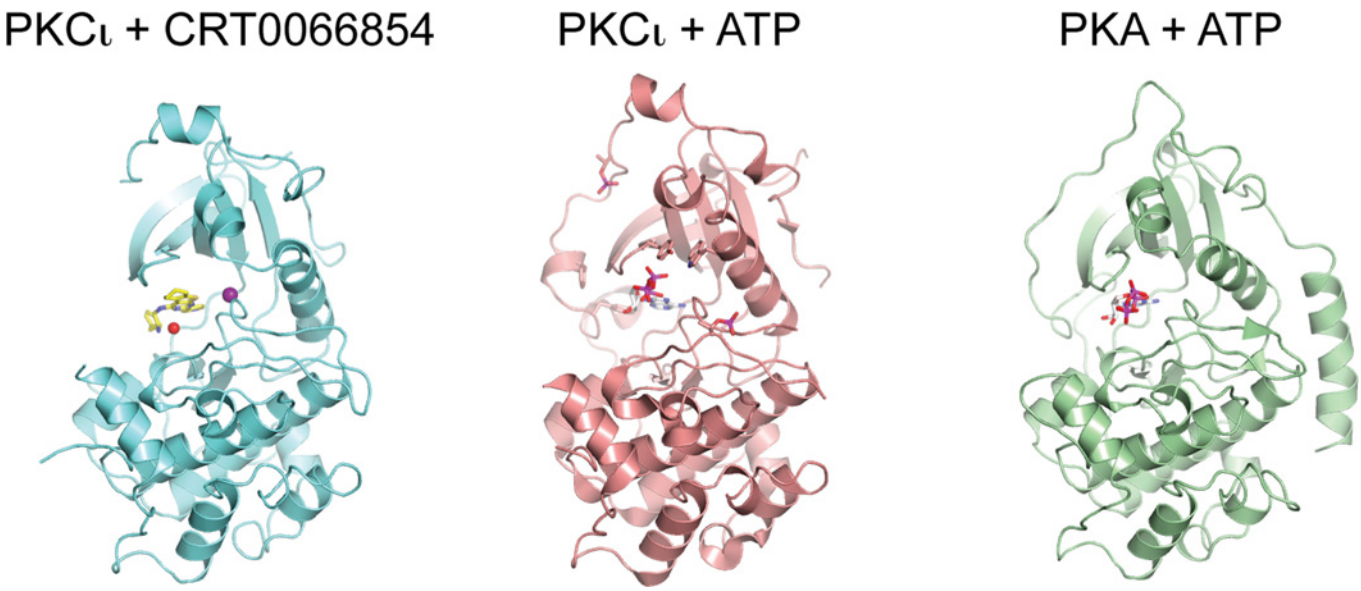

Figure S2 Structure of PKCι bound to CRT0066854 compared with PKCι bound to ATP and PKA bound to ATP

Overall fold of PKCι_K in complex with CRT0066854 (left-hand panel, cyan cartoon and yellow sticks), and ATP (middle panel, PDB code 3A8W, salmon-pink cartoon and sticks), with the PKA complex of ATP (right-hand panel, PDB code 1ATP, green cartoon and sticks) for comparison.

REFERENCES

1 Gassel, M., Breitenlechner, C. B., Konig, N., Huber, R., Engh, R. A. and Bossemeyer, D. (2004) The protein kinase C inhibitor bisindolyl maleimide 2 binds with reversed orientations to different conformations of protein kinase A. J. Biol. Chem. **279**, 23679–23690

2 Messerschmidt, A., Macieira, S., Velarde, M., Badeker, M., Benda, C., Jestel, A., Brandstetter, H., Neuefeind, T. and Blaesse, M. (2005) Crystal structure of the catalytic domain of human atypical protein kinase C-ι reveals interaction mode of phosphorylation site in turn motif. J. Mol. Biol. **352**, 918–931

Received 18 December 2012/12 February 2013; accepted 18 February 2013
Published as BJ Immediate Publication 18 February 2013, doi:10.1042/BJ20121871